DTU Library

Comparative assessment of typical control realizations of grid forming converters based on their voltage source behaviour

Vatta Kkuni, Kanakesh; Mohan, Sibin; Yang, Guangya; Xu, Wilsun

Published in:
Energy Reports

Link to article, DOI:
10.1016/j.egyr.2023.05.073

Publication date:
2023

Document Version
Publisher's PDF, also known as Version of record

Energy Reports 9 (2023) 6042–6062

Contents lists available at ScienceDirect

Energy Reports

journal homepage: www.elsevier.com/locate/egyr

Review article

Comparative assessment of typical control realizations of grid forming converters based on their voltage source behaviour

Kanakesh Vatta Kkuni [a], Sibin Mohan [b], Guangya Yang [a,*], Wilson Xu [c]

[a] Department of Electrical Engineering, Technical University of Denmark, Kgs. Lyngby, 2800, Denmark
[b] Quanta Technology, 2900 John Street, Unit 3, Markham, Ontario, Canada L3R 5G3
[c] Department of Electrical and Computer Engineering University of Alberta, Edmonton, Alberta, Canada T6G 2V4

ARTICLE INFO

Article history:
Received 20 August 2022
Received in revised form 3 May 2023
Accepted 18 May 2023
Available online 31 May 2023

Keywords:
Grid forming control inner loop
Small signal analysis
Virtual impedance
System stability

ABSTRACT

The generation of power system is transitioning from conventional synchronous generators with voltage source behaviour to power converter interfaced renewables. Power converters typically excel a current source behaviour, which fundamentally changes the dynamics of the power systems and resulting in stability challenges. To address these, a new type of control that can enable the converters to operate in a voltage source behaviour, referring to as grid forming control (GFC), is drawing significant interest from industry and academia. However, the reported control loops of the GFCs do not have a unified structure. Different control structures of GFC would lead to different pros and cons in different operational conditions based on their underlining control realization principles, the amount of parameters, and their setting rooms. Therefore, the stability augmenting voltage source behaviour cannot be considered as equal as for all the reported GFC realizations. This paper provides a critical review and discussion on the impact of inner control loop realizations of the GFC's reported in the literature on their stability during steady-state and large disturbances. Three typical GFC structures by inner loop controls based on, (1) cascaded voltage and current control, (2) inner current control, (3) no inner loop, are chosen for in-depth investigation. The analysis revealed that inner loops could negatively impact the voltage source behaviour of a GFC due to the complex control structure and the associated challenges of parameter tuning. The MW-level GFC with inner loops could potentially become unstable in a weak power system. Additionally, it is also revealed that GFC with cascaded control can operate stable for a narrow range of network impedance than other two types of controls. Furthermore, it is also shown that slow response behaviour based on cascaded inner loop can negatively impact dynamic reactive and active power-sharing and the fast-acting current limiting capabilities.

Contents

* Corresponding author.
E-mail address: gyy@elektro.dtu.dk (G. Yang).

https://doi.org/10.1016/j.egyr.2023.05.073

1. Introduction

In recent years, power systems in Europe and many places worldwide have seen a large increase in the use of Renewable Energy Sources (RES), and this trend is expected to continue, particularly in light of the energy crisis in Europe. Conventionally, renewable energy sources are integrated into the electric grid using power electronic (PE) inverters that are current-controlled. These current controlled principle is usually called as grid following converters (GFL) (Pattabiraman et al., 2018; Zarei et al., 2019; Poolla et al., 2019), which synchronizes with the grid through phase-locked loop (PLL) and regulates the phase angle of the output voltage to control the active and reactive currents flowing into the grid. In contrast, a conventional synchronous generator (SG), which was the key building block of the power system for decades has an inherent voltage source behaviour with predominantly low-frequency dynamics. Moreover, SG has a high overload capability compared to PE-based generators, which provides high short circuit power during the Such contrasting characteristics of SG and PE-based GFL can introduce severe challenges to the system stability as well as performance of the secondary equipment like protective relays due to different set of stability root causes and system dynamic characteristics (Milano et al., 2018; Markovic et al., 2019; Tielens and Van Hertem, 2016; Urdal et al., 2014; Homan et al., 2021; Ratnam et al., 2020; National Grid ESO, 2020). For instance, a study conducted by National Grid UK showed that 65% penetration of inverter-based generation in the UK grid could cause system-wide instability (Yu et al., 2015). Some of the specific challenges with increased PE interfaced resources, as identified by the European Network of Transmission System Operators, are Stojanovic et al. (2019)

- Reduced system inertia
- Reduced fast fault current contribution
- PE devices interact with each other and other passive components

Grid codes require the grid following converters in the transmission system to provide services such as fast frequency control and fast fault current injection to support the power system (ENTSO-E guidance document for national implementation for network codes on grid connection, 2017; Inertia2020 Working Group, 2020; National Grid Electricity System Operator, 2020). However, these services cannot fully compensate the missing intrinsic system inertia and short circuit power due to decommissioning of synchronous machines (Nationalgrideso, 2021). For example, although it is demonstrated that fast frequency support or synthetic inertia enabled by grid following inverter can improve the rate of change of frequency (RoCoF) during a disturbance (Rezkalla et al., 2018; Nguyen et al., 2017; Eriksson et al., 2017; Johnson et al., 2020), it requires accurate measurement of system frequency through PLL, thus dependent on a slow control loop compared to the instantaneous inertial response of synchronous generators (ENTSO-E, 2019; Liu et al., 2015). On the other hand, the fault current contribution from grid following converter is limited by the overload capability of the converter therefore cannot match the fault current magnitude from SG with the same power rating, which is often 3–5 times of its nameplate (Jia et al., 2018b; NERC, 2018; ENTSO-E, 2019). Moreover, it is a known issue that the dynamics of PLL play a big role in the control stability of the grid following inverter and is prone to instability in weak grids (Wen et al., 2013, 2015; Harnefors et al., 2007; Kkuni et al., 2019).

Deploying synchronous condensers (SCs), which is a type of synchronous machines that can provide limited inertia but full scale of short circuit current level, is a proven method to enhance the grid voltage source characteristics enabling higher penetration of RES. Several European projects have investigated and verified that the SC or SC combined with other components such as STATCOM or battery storage can compensate the deficiency in short circuit current and enhance the system inertia (SP Energy Networks, 2020; SCAPP, 2017; Nuhic et al., 2020). Studies have shown that optimal allocation of synchronous condensers can increase the short-circuit ratio (SCR) across the transmission system with enhanced reliability of the protection (Marrazi et al., 2018; Jia et al., 2018a). Another technology, which can potentially help address the challenges for the large scale integration of renewable sources, is to replace the control of some of the grid following converters via adding voltage source characteristics in the electrical response mimicking the behaviour of a synchronous generator in Zhong and Hornik (2012), Yu et al. (2015), Zhang (2010), Chen et al. (2020b), Lasseter et al. (2019) and Cheema (2020). This type of inverter is called Grid Forming Converter (GFC) or Virtual Synchronous Machine (VSM). The Ierna et al. (2016) and Denis et al. (2018) have shown that RES penetration limit could be potentially raised to 100% by deploying sufficient GFC in the transmission system. The advantages of Grid forming control in terms of inertial support have been demonstrated in the wind park and battery energy storage systems in MW level projects (ELectranet, 2021; Roscoe et al., 2019, 2020). In addition, strategic location of GFC in the network can enable sufficient voltage sources in the network thus allowing a reliable operation of system during system splits caused due to power system faults. In one of the first and latest attempts to define the requirements for a GFC, the UK system operator, National Grid, came up with the following requirements (National Grid ESO, 0000).

- Behave as a voltage source behind a constant Thevenin impedance in the frequency range of 5 Hz–1 kHz.
- Instantaneous response for faults and load changes
- Operate as a sink/source for harmonics and unbalance current.

It is expected that the requirements are similar from other utilities in Europe, given the guidelines from ENTSO-E (ENTSO-E, 2019). The requirement of GFC to behave as a voltage source behind a constant Thevenin impedance in the frequency range of 5 Hz–1 kHz is for the following reasons (ENTSO-E, 2019; Paolone et al., 2020),

- The passivity of the converter control characteristics will support the RMS models used in system studies.
- It prevents the adverse control interaction in a wide frequency range, thereby ensure highest possible stability in high frequency range.

However, operating GFC based on sensitive power electronic components implies that a robust current limitation method is needed, since GFC will not keep its voltage source behaviour or its internal emulated impedance. An impedance-based current limiting algorithm, which changes the internal impedance of the GFC dynamically to limit overcurrent during faults, has been identified as the most suitable current limitation method for the GFC (Paquette and Divan, 2014; Qoria et al., 2020; Liu et al., 2021; Taul et al., 2019). Impedance-based current limiting allows the GFC to maintain voltage source behind an impedance characteristic during large transients.

There has been significant research effort on GFC's recently (Yu et al., 2015; Ierna et al., 2019; Zhong and Hornik, 2012; Natarajan and Weiss, 2017; Zhong and Weiss, 2010; Rodriguez et al., 2013; Taul et al., 2019; Zhang et al., 2017; Remon et al., 2017; Li et al., 2019; Prevost and Denis, 2019; Wu and Wang, 2020; Qoria et al., 2020; Paquette and Divan, 2014; Li et al., 2019; Ma et al., 2017), which necessitates research effort on review, classification and comparative evaluation to fully understand and validate the pros and cons of different GFC realization methods. In Ratnam et al. (2020), a brief review and discussion on the existing inertia emulation control techniques available for GFC applications are reported. This paper also presents a few future research directions on GFC. Comprehensive review of inertial emulation and reactive power control of GFCs are reported in the literature (Tamrakar et al., 2017; Cheema, 2020; Chen et al., 2020b; Unruh et al., 2020; Rosso et al., 2021). Those studies focus on classifying and discussing various topologies of GFCs based on the inertial emulation loops, as well as the small signal and transient stability challenges of GFCs. However, they are purely review-based, which serves the purpose as a compilation of the recent technological development, however provide no independent stability or time-domain analysis to evaluate the voltage source characteristics. In addition, the focus of these papers are on the outer loops of GFC, which includes inertial emulation and reactive power control. The impact of inner control loops, such as voltage and current control, present in several GFC topologies have not been considered. However, inner loops can play a significant role in MW level converters with low switching frequency. The possibility of GFC negatively interacting with an existing SG in the system is also not assessed in these papers.

From stability assessment point of view, existing literature does not contain detailed small-signal analysis and interaction study with SG, with no considerations on the impact of inner loops (Liu et al., 2015; Sun et al., 2020). Qu et al. (2020) studies the impact of a cascaded voltage and current control-based inner loop of the GFC using small-signal models. However, the study only considers one type of the GFCs based on inner loop realizations. The paper also does not address the interaction between an SG and the inner loop of a GFC.

Based on the reported GFCs, yet another way to classify the GFCs is based on the realization methods, whether it is based on inner control (current management) structures or outer loop structures. The outer loop structures for GFC are usually based on virtual impedance, droop, or virtual synchronous machine methods. For inner loop realization methods, three common topologies based on different inner loop structures have been widely reported in the literature (i) without any inner loop current control, (ii) with inner loop current control, (iii) with inner current control and cascaded voltage control. There are opposing arguments presented in literature about the benefits of each of these topologies. Some studies recommended that inner loop controllers such as valve current controller and PCC voltage controllers are required as the power electronic converters are sensitive to disturbances, and it is easier to implement the current limits on converters with inner loops. Furthermore, the inner loops can provide additional damping for the filters (Taul et al., 2019; Qu et al., 2020). Whereas, the other studies mentioned that inner controller loops are not recommended, because (i) it can impair the instantaneous response time of the GFC (ii) the presence of controller could cause undesirable controller interactions and thus unstable operation (Yu et al., 2015). Furthermore, some latest studies conclude that an increase in grid impedance is better for the stability of the GFC with cascaded voltage control which is in contrast to the behaviour of an SG or an ideal GFC (Du et al., 2019; Qu et al., 2020; Li et al., 2020). As opposing arguments are presented in literature, a detailed comparative analysis of various GFC topology is required to clarify the pros and cons of different methods, especially from dynamics point of view. In addition, the performance of current limitation algorithms in these GFC types also needs to be analysed to study how different inner loops impact on the design and characteristics of the current limiters of the GFC.

The existing literature on grid forming control (GFC) based on inner loops has several deficiencies, which creates a clear gap for a critical review of the three prevalent GFC topologies, particularly for MW level converters connected to the transmission systems. To provide a fair comparison, such a review needs to be supplemented by a detailed implementation of small-signal and time-domain analysis. In this context, the comparative analysis and the results presented in this paper can provide a clearer understanding of the effects of the three prevalent inner loops on an MW level GFC. In addition, impedance based on the current limitation strategy, where the internal impedance of the GFC is changed dynamically to limit the current during system faults, is realized for all three configurations in this paper. In addition, the results of the time-domain performance of the analysed GFC types are presented to evaluate the current limitation performance. A comparison between this paper and already existing review papers on GFC are shown in Table 1.

The main contributions of this paper are summarized as,

- Small signal models of three GFC configurations based on inner loop realizations are developed, and a small signal study is conducted to identify the impact of inner loops of MW level GFC.
- Dynamic impedance assessment of GFC is conducted to identify non-negative resistance regions.
- Small signal analysis to study inner loop impact on the electromechanical mode of an SG is presented.
- Comparative evaluation of the impedance based current limitation of the studied GFC configurations is reported.

Table 1
A comparative summary of this study and previous review on GFC.

Paper	Small signal modelling	Evaluates all inner loop types	Inner loops stability impact	Interaction with SG	Response evaluation	Grid strength sensitivity
Ratnam et al. (2020)	×	×	×	×	×	×
Tamrakar et al. (2017)	×	×	×	×	×	×
Cheema (2020)	×	×	×	×	×	×
Chen et al. (2020b)	×	×	×	×	×	×
Unruh et al. (2020)	×	×	×	×	×	×
Rosso et al. (2021)	×	×	×	×	×	×
Liu et al. (2015)	✓	×	×	✓	×	×
Sun et al. (2020)	✓	×	×	✓	×	×
Qu et al. (2020)	✓	×	✓	×	×	✓
This study	✓	✓	✓	✓	✓	✓

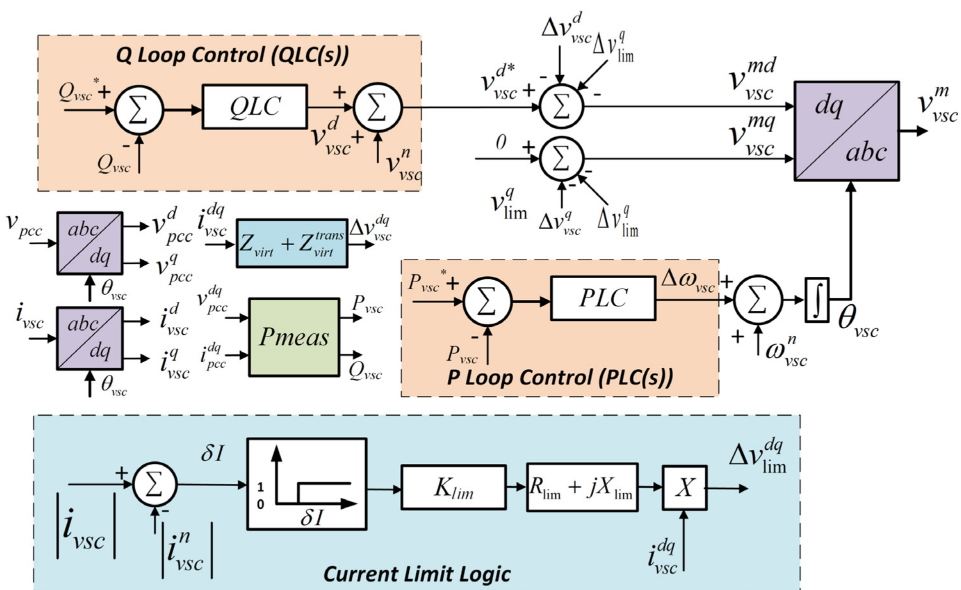

Fig. 1. General Control System of GFC without an inner loop.

- Case studies are presented based on time-domain analysis to validate the small-signal analysis and compare the performance of GFCs.

The remaining section of paper is organized as the following. Section 2 describes three targeted inner loop control methods for GFC. Section 3 focuses on the entire of the converter control system and the small signal models. In Section 4 the small signal model of the entire system is presented, followed by the analysis and validation in Section 5. Time-domain simulation study is presented in Section 6 followed by summary in Section 7. Conclusion and discussions are presented in Section 8.

2. System description

A GFC is expected to behave like a voltage source behind an impedance. Where a reactive power loop determines the voltage amplitude and the inertia loop sets the phase angle of the voltage. There are predominantly three inner control methods for realizing the voltage source characteristics of a GFC, which are

- GFC structure implemented without any inner current or voltage control and transient and steady state virtual impedance as shown in Fig. 1 (Yu et al., 2015; Ierna et al., 2019; Zhong and Hornik, 2012; Natarajan and Weiss, 2017; Zhong and Weiss, 2010). The control is equipped with virtual impedance based current limit method described in Paquette and Divan (2014) and Qoria et al. (2020).
- GFC structure implemented with an inner current control and transient virtual impedance, with the current references generated by a virtual dynamic admittance as shown in Fig. 2 (Rodriguez et al., 2013; Taul et al., 2019; Zhang et al., 2017; Remon et al., 2017; Li et al., 2019). The control is equipped with virtual impedance based current limit method described in Liu et al. (2021).
- GFC structure implemented with cascaded voltage and current control and transient and steady state virtual impedance as shown in Fig. 3 (Prevost and Denis, 2019; Wu and Wang, 2020; Qoria et al., 2020; Paquette and Divan, 2014; Li et al., 2019; Ma et al., 2017; Shi et al., 2020). The control is equipped with current limitation method described in Taul et al. (2019).

A two-source model, as shown in Fig. 4 consisting of an SG, GFC, transmission line (Z_{TL1}, Z_{TL2}), load(Z_{Load}) and transformer (Z_{T1}) is the system used to conduct the stability and time domain analysis in this paper. This system is sufficient enough also to capture the dynamic interaction between an SG and GFC while allowing to draw definite conclusions (Collados-Rodriguez et al., 2019). The passive components of the studied system are described in Table 2. The GFC filter is modelled by a reactor

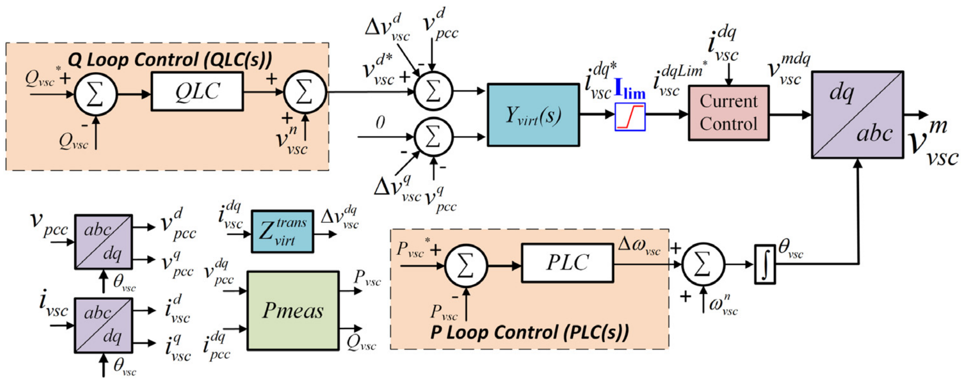

Fig. 2. General Control System of GFC with current control inner loop and virtual admittance.

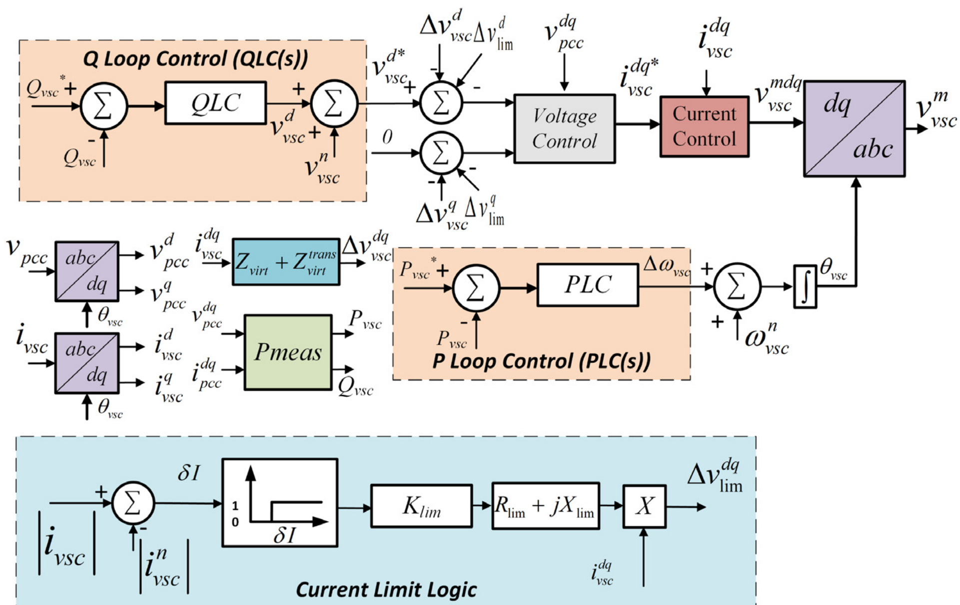

Fig. 3. General Control System of GFC with cascaded voltage and current control inner loop.

Table 2
Components of the two-source model in Fig. 4.

Parameter	Description (pu)
L_1	Filter reactor
R_1	Resistance filter reactor
C_f	Filter capacitor
R_f	Damping resistance
Z_{T1}	Impedance of VSC transformer
Z_{Load}	Load impedance
Z_{TL1}	Transmission line impedance between load and GFC
Z_{TL2}	Transmission line impedance between SG and GFC

$L1$, and its loss resistance $R1$, capacitance filter C_f and damping resistor Rf. The network includes passive network impedance, filters, transformers and the load modelled as a resistance. The transformer and network impedance is modelled as resistive inductive (RL) equivalent.

The full system is modelled in a rotating reference frame for small-signal analysis. The network, including the filter reactor, capacitance, load, and the grid impedance, is modelled in D-Q frame, which is defined by the speed of the synchronous machine and is aligned with the swing bus terminal voltage (v_{sg}). The VSC is modelled in a d-q frame (d-q frame) defined by the VSC's power loop output ω_{vsc}. In the rest of the paper, all lowercase variables with an appended superscript of D or Q represent the D or Q component of the original parameter defined in the D-Q frame. At the same time, all lowercase variables with an appended superscript of d or q represent the d or q component of the actual parameter described in d-q frame. For instance, i_{vsc}^{D} represents the direct axis component of the VSC current in DQ frame. Variable superscripted with d-q or DQ is variable vectors of the direct and quadrature frame original parameters represented in the dq or the DQ frame, depending on the superscript. Also, the variable with appended '0' represents the steady-state value of the parameter.

A commonly used four winding electrical network representation of a salient pole synchronous machine (Kundur, 1994), along with a simplified automatic voltage regulator (AVR) and speed Governor (GOV) used for the study. The simplified AVR model consists of cascaded PI control and a low pass filter which forms the excitation system model.

$$G_{AVR} = \frac{Kp_{AVR}s + Ki_{AVR}}{s} * \frac{1}{1 + sT_{AVR}} \tag{1}$$

where T_{AVR} is the time constant. The simplified governor is realized by a simplified model emulating a first order response with

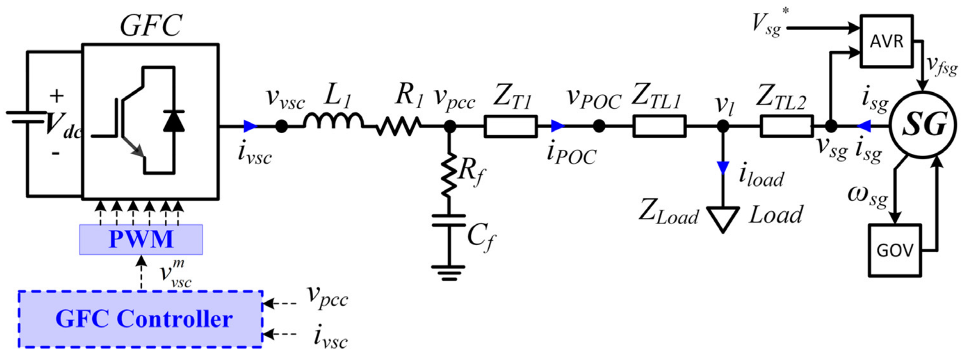

Fig. 4. Simplified one-line diagram of studied system.

a f-p droop.

$$G_{gov} = \frac{1}{R} * \frac{1}{1 + sT_{gov}} \tag{2}$$

where R is the p-f droop expressed in p.u. In this study, it is chosen to be same as that of GFC at 0.05 p.u.

3. GFC control system and small signal modelling

This section describes the control system of the GFC's considered in this paper and small signal modelling. The GFC control structures analysed in this paper is shown in Figs. 1–3. The converter control system studied in this paper, is implemented in a synchronously rotating reference frame (d-q frame) defined by ω_{vsc} (dq). In all the GFC structures considered in this paper, the voltage and current parameters are first transformed into (d-q frame) using a frame transformation matrix T_{vsc}. The transformation blocks, active and reactive power loops and power measurement blocks are common for the three GFC types are discussed in this section. The following simplifications/assumptions are made in this study for the sake of easier understanding

- DC link dynamics is neglected.
- The power converter configuration is assumed to be a simple 2 level VSC
- The network and events are considered to be balanced
- The zero sequence network is not modelled in small-signal analysis, as only a balanced network is considered. Furthermore, the transformer, Z_{T1} is of delta/star winding, thus zero sequence current is blocked.
- Transmission lines are substituted with its RL equivalents.
- The excitation field winding limiters are neglected
- The mechanical shaft of the SG is modelled as a single mass model.

3.1. GFC control system components

The control components of the GFC controls and their linear models are described below.

3.1.1. Reactive power loop, Q loop control (QLC(s))

The GFC are voltage sources with a nominal voltage of v_{vsc}^n. A reactive power slope, *Kslope* is employed for steady state reactive power sharing.

$$QLC = Kslope * \frac{1}{1 + sT_{QLC}} \tag{3}$$

A typical value of 5% is chosen for *Kslope* and 0.5 s time constant is chosen for reactive power loop parameters.

3.1.2. Active power loop, P loop control (PLC(s))

The active power control emulates the electromechanical behaviour, which also sets the phase angle of the emulated voltage source. The implementation for the power loop controller could vary substantially depending on the amount of damping and inertia output required from the GFC (Sun et al., 2020). For instance, the active power controller can be a simple gain to provide a response similar to a conventional P-f droop or a second-order function to mimic the inertial constant of a synchronous machine. The active power controller is realized as a cascaded combination of gain and low pass filter as given in Eq. (4), which mimics the swing equation of a synchronous machine.

$$PLC = R * \omega_b * \frac{1}{1 + sT_{inert}} \tag{4}$$

where are R is the P-f droop represented in p.u with a typical value of 0.05, and ω_b is the base frequency in rad/s, and emulated inertial constant can be written as

$$H = \frac{T_{inert}}{R} \tag{5}$$

This paper sets the inertia constant and droop gain as 6 s and 5%, respectively.

3.1.3. Virtual impedance and transient virtual impedance (Z_{virt}, Z_{virt}^{trans})

The electrical model of the GFC without inner loop as shown in Fig. 1 and for GFC with cascaded control shown in Fig. 3 are realized by implementing a Virtual impedance and transient virtual impedance ($Z_{virt}, Z_{virt}^{trans}$) in the GFC control system. The virtual impedance block emulates the static voltage drop across a resistive and inductive circuit. The transient virtual impedance, Z_{virt}^{trans}, realized by a high pass filtered current, is typically resistive to provide enough damping for the network resonance modes (Zhang, 2010). The high pass filter cutoff frequency should cover most sub-synchronous frequencies to eliminate the network resonance modes. The combined realization of virtual and transient virtual impedance is shown in Eq. (6).

$$\Delta v_{vsc}^{dq} = \underbrace{(R_{virt} + j\omega_b L_{virt})}_{Z_{virt}} i_{vsc}^{dq} + \underbrace{(R_{virt}^{trans} * H_{hp}(s))}_{Z_{virt}^{trans}} i_{vsc}^{dq} \tag{6}$$

where v_{vsc}^{dq}, and i_{vsc}^{dq} are the voltage and current at the inverter terminals. $H_{hp}(s)$ is the high pass filter represented as

$$H_{hp}(s) = \frac{s\tau_{hp}}{(1 + s\tau_{hp})} \tag{7}$$

It has to be noted that the parameters of the virtual impedances are different for the case with cascaded inner control and GFC without inner loop control because for the GFC with the cascaded case, the voltage is controlled at the PCC, and for no inner loop case the voltage is controlled at the converter terminal.

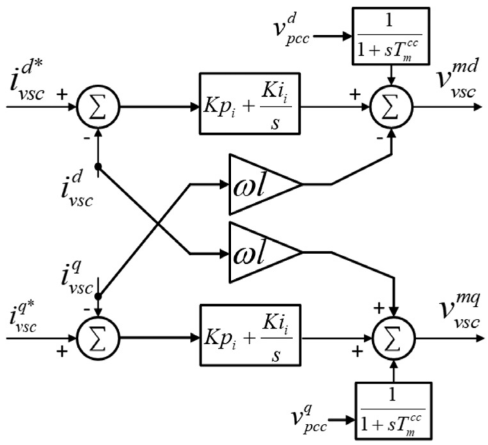

Fig. 5. Decoupled dq current controller.

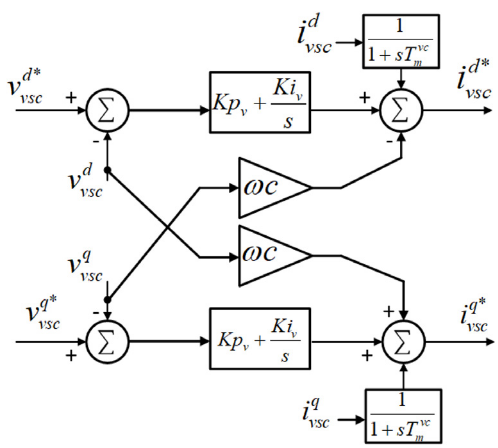

Fig. 6. Decoupled dq voltage controller.

3.1.4. Virtual admittance ($Y_{virt}(s)$)

The virtual admittance is utilized in the GFC control with only current control inner loop as shown in Fig. 2. The virtual admittance is used to create the current references from the terminal voltage and PCC voltage as shown in (8)

$$i^{dq*}_{vsc} = \frac{v^{dq}_{vsc} - v^{dq}_{pcc}}{(R_{virt} + sL_{virt} + j\omega L_{virt})} \tag{8}$$

where v^{dq}_{pcc} is the pcc voltage of the GFC.

3.1.5. Current controller

A decoupled dq current control as shown in Fig. 5 is utilized in both GFC with current control and GFC with cascaded control.

The control is implemented in dq frame, T^{cc}_m is the time constant of the feed forward filter, the decouple term ωl is given in (9).

$$\omega l = \omega_{ref}(L_1) \tag{9}$$

3.1.6. Decoupled voltage controller

The decoupled voltage controller is implemented for the GFC with cascaded control loops, as shown in Fig. 6

The decoupling term is defined as

$$\omega c = \omega_{ref}(C_f) \tag{10}$$

The time constant of the feed forward filter is T^{vc}_m.

3.1.7. Power measurement block (Pmeas)

The power measurement block is used in all the GFC's discussed in this paper. The *Pmeas* block computes the active and reactive power as in (11) and (12)

$$P_{vsc} = v^D_{vsc} i^D_{vsc} + v^Q_{vsc} i^Q_{vsc} \tag{11}$$

$$Q_{vsc} = v^Q_{vsc} i^D_{vsc} - v^D_{vsc} i^Q_{vsc} \tag{12}$$

The linearized form of the power measurement block is

$$\Delta P_{vsc} = v^{D0}_{vsc} \Delta i^D_{vsc} + v^{Q0}_{vsc} \Delta i^Q_{vsc} + \Delta v^D_{vsc} i^{D0}_{vsc} + \Delta v^Q_{vsc} i^{Q0}_{vsc} \tag{13}$$

$$\Delta Q_{vsc} = v^{Q0}_{vsc} \Delta i^D_{vsc} - v^{D0}_{vsc} \Delta i^Q_{vsc} + \Delta v^Q_{vsc} i^{D0}_{vsc} - \Delta v^D_{vsc} i^{Q0}_{vsc} \tag{14}$$

3.1.8. Frame transformation matrix (T_{vsc})

The non-linear transformation matrix (T_{vsc}) is utilized to translate the variables to the dq reference frame, in which the GFC control is implemented. The linearized form of the transformation matrix is a function of the steady-state value of the transformed variable and the angle difference between the two frames. In addition to the original input variables, the linearized T_{vsc} also has additional input variable $\Delta\theta_{vsc}$. The linearized equation for frame transformation matrix T_{vsc} is given by

$$\Delta x^{dq} = T_{vsc}(x^{D0}, x^{Q0}, \Delta\theta_0)[\Delta x^{DQ}, \Delta\theta_{vsc}]^T \tag{15}$$

where, x^{dq} are the variables in VSC controller reference frame, x^{DQ} are the variables in the common reference frame and T_{vsc} is function of steady state operating point and is given by

$$T_{vsc} = \begin{bmatrix} \cos(\theta_0) & -\sin(\theta_0) & -x^{Q0}\sin(\theta_0) - x^{D0}\cos(\theta_0) \\ \sin(\theta_0) & \cos(\theta_0) & x^{D0}\cos(\theta_0) - x^{Q0}\sin(\theta_0) \end{bmatrix} \tag{16}$$

Similarly, the linearized transformation of variables in dq frame to DQ frame is given by

$$\Delta x^{DQ} = T^{-1}_{vsc}(x^{d0}, x^{q0}, \Delta\theta_0)[\Delta x^{dq}, \Delta\theta_{vsc}]^T \tag{17}$$

where,

$$T^{-1}_{vsc} = \begin{bmatrix} \cos(\theta_0) & \sin(\theta_0) & -x^{q0}\sin(\theta_0) + x^{d0}\cos(\theta_0) \\ -\sin(\theta_0) & \cos(\theta_0) & -x^{d0}\cos(\theta_0) - x^{q0}\sin(\theta_0) \end{bmatrix} \tag{18}$$

The angle difference θ_0 between the reference frames is given as

$$\theta_0 = (\Delta\omega_{sg} - \Delta\omega_{vsc})/s \tag{19}$$

3.1.9. PWM and computation delay

To account for the PWM and computation, a delay corresponding to switching frequency has to be accounted. The delay *Td*, is chosen considering a single updated PWM (Harnefors et al., 2015). A third order Pade approximation of the delay is used for small signal state space analysis.

3.1.10. Current limit logic

A current limit logic based on increasing the internal impedances is incorporated in the GFC's studied in this paper. The impedance-based current limit can maintain the voltage source behind the impedance nature of the GFC, albeit with increased internal impedances. The implementation of the impedance based current limit and its advantages are discussed in Paquette and Divan (2014) and Qoria et al. (2020). The impedance based current limit is applicable to all the studied GFC types. For the GFC with no inner loop and cascaded control, the impedance current limit is as shown in Figs. 1 and 3. The additional internal virtual

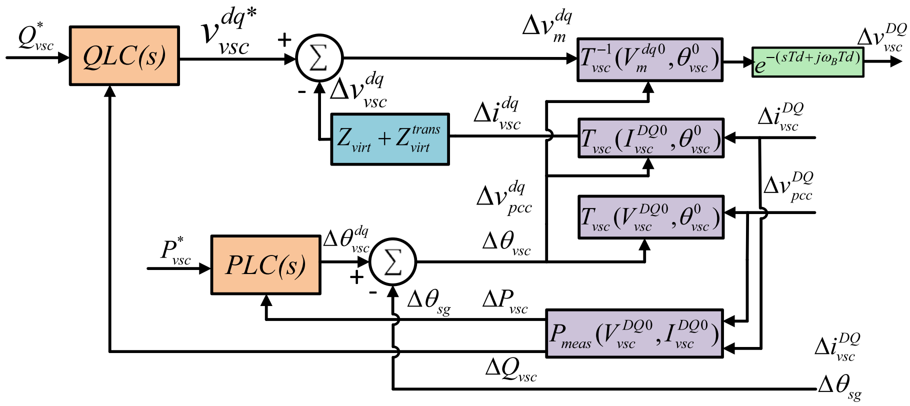

Fig. 7. Small signal model of the GFC with no inner loop.

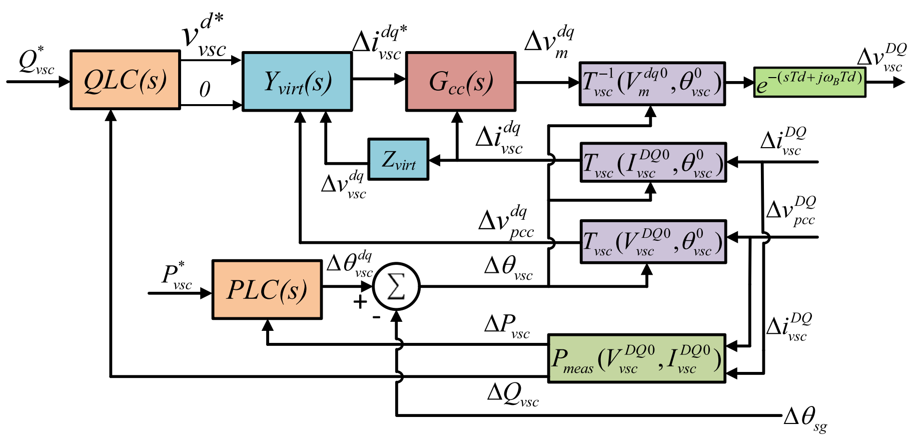

Fig. 8. Small signal model of the GFC with current control inner loop.

impedance, $Z_{\lim}$, active during over current scenario where the output current exceeds the nominal rated current I^n_{vsc}, is given by

$$Z_{\lim} = \begin{cases} K_{\lim} Z_{\lim} & \text{if } \delta I > 0 \\ 0 & \text{if } \delta I \le 0 \end{cases} \tag{20}$$

Where δI is the difference in magnitude between the measure output current of the GFC and nominal current. For GFC with only current control and virtual admittance the current limit is realized as

The limited current vector i^{dqLim*}_{pcc}

$$i^{dqLim*}_{vsc} = \frac{1}{KC_{lim}} * I^{dq*}_{vsc}, \text{ where } KC_{lim} = \frac{\left|I^{dq*}_{vsc}\right|}{I^n_{vsc}} \tag{21}$$

In the case of GFC with only current control, although the internal impedance during current limit operation is not changed direction, but it is indirectly adjusted to achieve the current limits as discussed in Cunha et al. (2021)

3.2. Small signal model of GFC's

The small-signal model derived in either stationary reference or synchronously rotating reference frame is sufficient for impedance-based stability analysis (Wang et al., 2017). However, the study also employs other small-signal analysis methods such as eigenvalue and participation factors, which are more efficiently done in a rotating reference frame where a steady-state value exists. In addition, the synchronous machine model is typically developed in the dq reference frame, Kundur (1994), and the converter control studied in this paper is also implemented in the dq reference frame. Thus the small-signal model of the system studied in this paper is derived in the rotating reference frame.

The small-signal model of the GFC's developed by interconnecting the linear model of each of the control components of GFC explained in the above subsections based on matching input and output signals. The current limit logic only acts in the over-current scenario and thus is not considered in the small-signal modelling. The small-signal model of the GFC without an inner loop is shown in Fig. 7. Similarly the small-signal model of the GFC with cascaded voltage and current control and GFC with only inner current control is shown in Figs. 8 and 9 respectively.

The $G_{cc}(s)$ is the current controller transfer function as shown in Fig. 5, and $G_{vc}(s)$ is the voltage controller as shown in Fig. 6.

4. Modelling methodology and analysis overview

An overview of the modelling and analysis conducted in the subsequent section of the paper is presented in this section. Furthermore, the parameters for the comparative analysis are also shown in this section.

Firstly, to ensure a fair comparison, the three GFC models should have the same steady-state performance. As presented in the previous section, the controller structures are different for the three GFC models. For instance, the GFC with the cascaded control loop regulates the voltage at PCC or the GFC filter bus (v_{pcc}), whereas the GFC with no inner loop controls the inverter terminal voltage (v_{vsc}). On the other hand, the GFC with current control regulates the voltage at a virtual point defined by the virtual admittance ($Y_{virt}(s)$). Therefore, in addition to ensuring the parameters of active and reactive power loops to be the same,

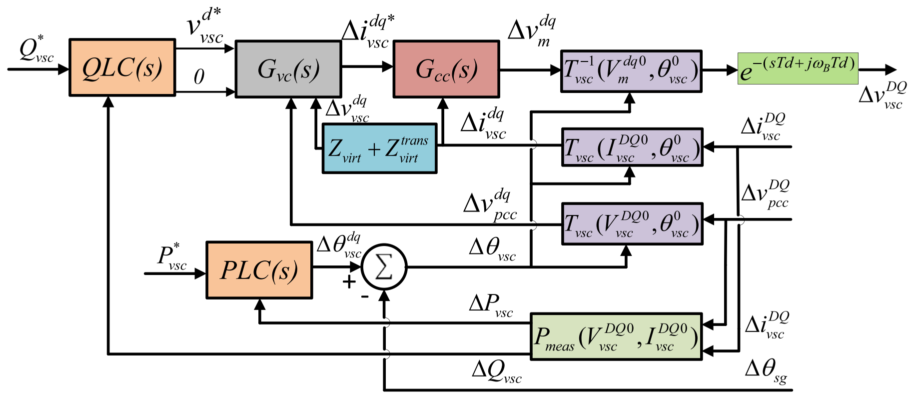

Fig. 9. Small signal model of the GFC with cascaded voltage and current inner loop.

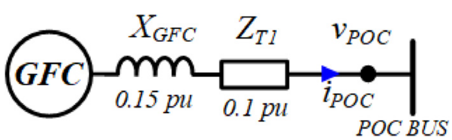

Fig. 10. Simplified electrical equivalent circuit of the considered GFC's.

Table 3
GFC's virtual impedance or admittance for the base case.

GFC type	Parameter	Per-unit (pu)
GFC no inner loop	Z_{virt}	$-0.05j$
GFC with current control	$Y_{virt}(s)$	$\frac{1}{s*0.15+0.15j}$
GFC with cascaded control	Z_{virt}	0.15j

Table 4
GFC filter and network parameters for the base case scenario.

Parameter	Per-unit (pu)	Parameter	Per-unit (pu)
L_1	0.2	R_1	0.02
R_f	0.3	C_f	0.05
Z_{TL1}	0.01 + 0.1j	Z_{TL2}	0.02 + 0.2j
Z_{T1}	0.1j	Z_{Load}	1.0

each of the GFC's virtual impedance or admittance are designed to provide the same steady-state characteristics when the outer power loops are kept open. In this study, GFC's virtual impedance or admittance is designed such that the steady-state reactance of all GFC's (X_{GFC}) are 0.15 pu with an equivalent circuit as shown in Fig. 10. The values of virtual impedances or admittance chosen for the base case scenario is shown in Table 3.

4.1. Parameters of the GFC for the comparative analysis

Firstly, a base case scenario is defined to compare against cases with parameter variations. The base case switching frequency is 2 kHz which is typical for MW level systems. The filter parameters are designed for the base case switching frequency of 2 kHz. The electrical parameters of the system in Fig. 4 are for the base case scenario, represented in per unit at a base power of 70 MVA and voltage of 13.8 kV are shown in Table 4.

The current control parameters for the GFC with current control are designed to meet a 5 ms rise time for the base case. Furthermore, to ensure reduced transients during network voltage changes, an upper constraint of 5 ms is considered for the voltage feed-forward filter (T^{cc}_m) in the tuning process. To emphasize the importance of switching frequency, a second case

Table 5
Control Designs considered for cascaded control based GFC.

Design 1	PWM delay (T_d) = 0.5 ms Voltage control time constant = 20 ms Current control time constant = 5 ms voltage feed forward filter (T^{cc}_m) $\leq$ 5 ms
Design 2	PWM delay (T_d) = 0.1 ms Voltage control time constant = 20 ms Current control time constant = 1 ms voltage feed forward filter (T^{cc}_m) $\leq$ 5 ms
Design 3	PWM delay (T_d) = 0.1 ms Voltage control time constant = 20 ms Current control time constant = 1 ms

with the GFCs switched at 10 kHz is also studied in this paper. While such high switching frequency is not typical for MW level converter, this analysis is necessary to study the impact of switching frequency and thereby understand how well the conclusion from past studies conducted at kW level GFCs at microgrid level translate to MW level systems. For the case with a GFC switching at a frequency of 10 kHz, the rise time of the current control response for the GFC is decreased to 1 ms from 5 ms.

For GFC with cascaded control, the control design is conducted to meet three different control design objectives, as shown in Table 5. The first design with GFC switching at 2 kHz is shown in the Table 5 is the base case for GFC with cascaded control. The different designs are chosen to analyse the impact of control design methodologies. To ensure better transient performance, an upper constraint on the time constant is placed on the voltage feed-forward low pass filter time constant on the first two design objectives. The control design is carried out with the network parameters specified in Table 4, and the performance could vary if the network parameters change, which is also investigated in this paper.

4.2. Small signal modelling methodology

The small-signal model of the three major building blocks, the GFC, SG and the Network, are formed individually and subsequently interconnected with the respective input output characteristics. The small-signal model of each of the three GFC's which are derived in dq frame, are then interconnected to the rest of the system modelled in DQ frame using transformation matrices defined in Eqs. (15) and (17). The network model also includes the converter filters and the transformer impedance, load and network impedance. The linear model of the synchronous machine is well established (Kundur, 1994) and therefore not shown in

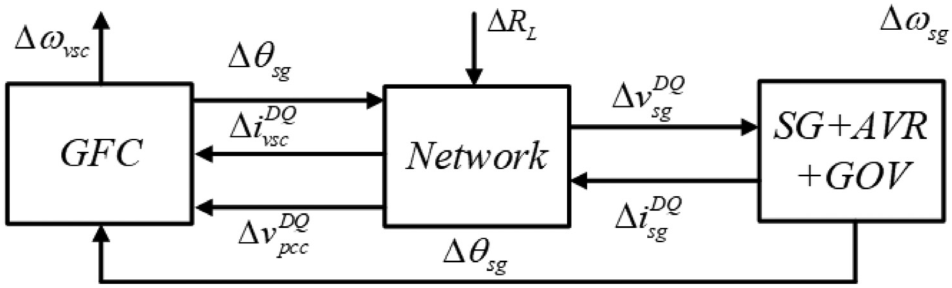

Fig. 11. Small signal modelling methodology of the system.

this paper. The outline of the interconnection of the small signal model of the system is shown in Fig. 11. The current limitation algorithm only acts during over current initiating events and thus is not included in the small-signal modelling and analysis.

4.3. Impedance analysis and passivity of GFC's

The impedance-based analysis, a valuable tool for analysing the stability of interconnected power components, is used to study the characteristics of the GFC's considered in the paper. Insightful information about the system's dynamic characteristics can be derived simply by analysing the dynamic impedance of the system (Suntio et al., 2017). The dynamic DQ frame impedance of the GFC's are calculated at the POC terminal and is defined as the transfer function between the voltage and current at the POC, as shown in Eqs. (22) and (23).

$$Vpoc_{DQ}(s) = Z_{DQ}(s) * Ipoc_{DQ}(s) \tag{22}$$

where

$$Z_{DQ}(s) = \begin{bmatrix} Z_{DD}(s) & Z_{DQ}(s) \\ Z_{QD}(s) & Z_{QQ}(s) \end{bmatrix} \tag{23}$$

A DQ frame impedance for passive components has high off-diagonal elements due to coupling. Therefore, a modified positive–negative sequence impedance, which is diagonally dominant (Rygg et al., 2016) and expressed in DQ domain as shown in Eqs. (24) is used in this study to analyse the GFC impedance.

$$\begin{bmatrix} V_p \\ V_n \end{bmatrix} = \begin{bmatrix} Z_{pp}(s) & Z_{pn}(s) \\ Z_{np}(s) & Z_{nn}(s) \end{bmatrix} \begin{bmatrix} I_p \\ I_n \end{bmatrix} \tag{24}$$

$$Z_{pn} = \begin{bmatrix} Z_{pp}(s) & Z_{pn}(s) \\ Z_{np}(s) & Z_{nn}(s) \end{bmatrix} \tag{25}$$

$$Z_{pn} = A_Z.Z_{DQ}.A_Z^{-1}$$
$$A_Z = \frac{1}{\sqrt{2}} \begin{bmatrix} 1 & j \\ 1 & -j \end{bmatrix} \tag{26}$$

The Passivity Theorem could be applied to analyse the VSC input impedance behaviour (Harnefors et al., 2007; Agbemuko et al., 2020) and understand potential instability. A passive system can only dissipate the energy and cannot produce energy, thus an interconnected network composed of passive impedances, such as RLC network are passive and will never be unstable. In the frequency domain, the dynamic impedance is passive if,

$$Z_{pn}(j\omega) + Z_{pn}^H(j\omega) > 0, \forall\omega \in R \tag{27}$$

Where H is the Hermitian operator. The left hand side of (27) can be equated to

$$Z_{pn}(j\omega) + Z_{pn}^H(j\omega) = \begin{bmatrix} A & C^* \\ C & B \end{bmatrix} \tag{28}$$

Where,

$$\begin{aligned} &A = 2\mathrm{Re}\{Z_{pp}(j\omega)\}, B = 2\mathrm{Re}\{Z_{nn}(j\omega)\} \\ &CC^* = (Z_{pn}^*(j\omega) + Z_{np}(j\omega))(Z_{np}^*(j\omega) + Z_{pn}(j\omega)) \end{aligned} \tag{29}$$

To check if the impedance is dissipative or passive, a simple positivity check could be done.

$$A > 0, B > 0, AB > CC^* \tag{30}$$

The modified sequence domain impedance is diagonally dominant, and hence the passivity could be verified simply by ensuring a positive real part of $Z_{pp}(jw)$ for all frequencies. However, it should be noted that no power converter impedance can remain passive over the entire frequency range, as will be explained later in the paper.

5. Small signal analysis

The small-signal model of the full system shown in Fig. 4 for all the three GFC configurations is developed by interconnecting linear dynamical models of GFC, SG, and the network. Analysis conducted on the derived small-signal model of the GFC system, including impedance and passivity analysis and eigenvalue analysis, is presented in this section. The current limitation algorithm is not included in the small signal analysis.

5.1. Model verification

The three separate linear models of the complete system with the considered GFC are Verified against the nonlinear time-domain model shown in Fig. 4. The response of the full system model with no inner loop-based GFC for 5% step change in the load at 7 s and 5% step change in the reference power at 10 s is shown in Fig. 12. The response of the system for the same events with cascaded control loop based GFC and inner current control based GFC are shown in Figs. 14, and 13 respectively. These figures show that the developed linear model provides the same transient response as the nonlinear model, thus confirming the developed linear model's accuracy.

5.2. Impedance characteristics without the outer active and reactive power loop

The GFC is expected to provide a response similar to that of a voltage source behind an impedance for load changes and faults and to behave as a passive impedance between 5–1 kHz. Furthermore, the impact of virtual impedance on the output impedance also needs to be assessed. Therefore, a dynamic impedance assessment of the GFCs without considering the outer loops is carried out to derive insightful information on the impedances of the GFC. The comparison of the GFC's output impedance ($Z_{pp}(s)$)

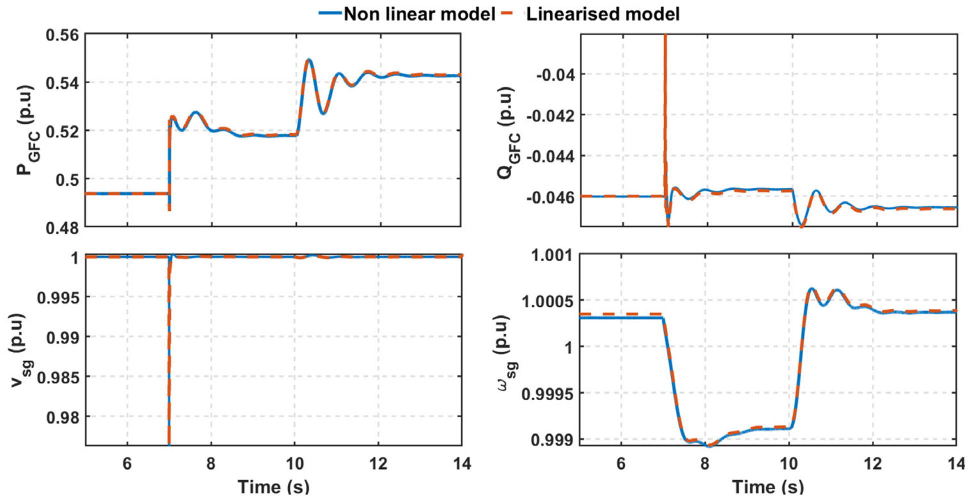

Fig. 12. Verification of system model with no inner loop based GFC.

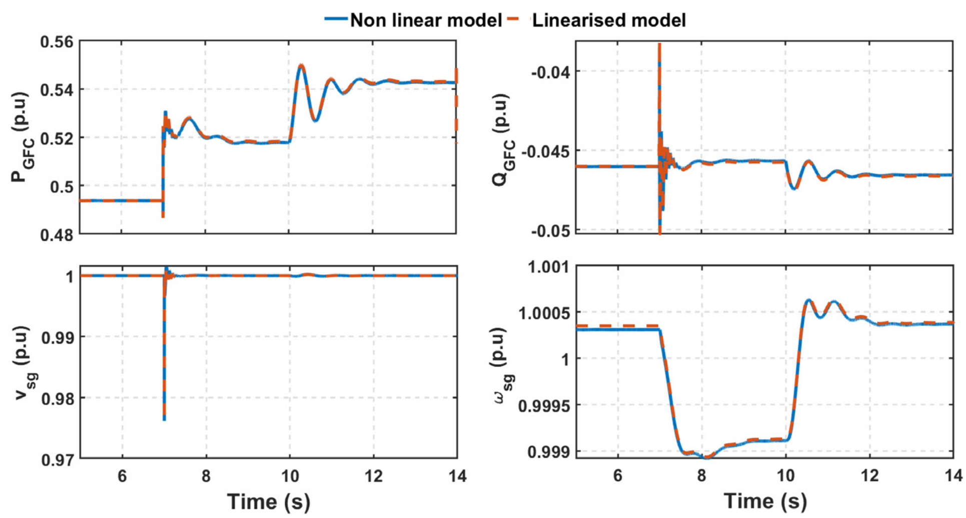

Fig. 13. Verification of system model with current control loop based GFC.

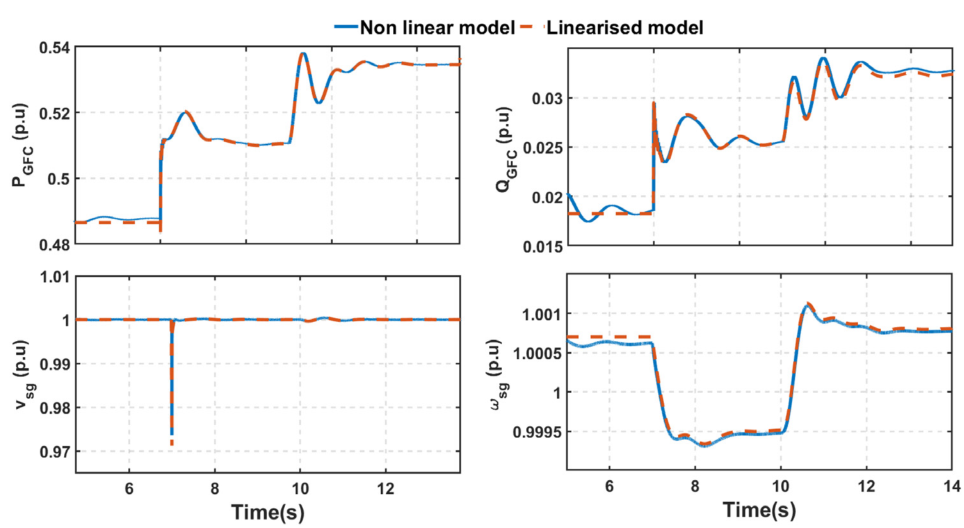

Fig. 14. Verification of system model with cascaded control loop based GFC.

at POC is shown in Fig. 15. The impedance of an ideal voltage source with 0.15 pu reactance for X_{GFC} is also plotted in Fig. 15. At very low frequencies, all the GFCs have similar impedance as expected. However, it is seen that the GFC with cascaded control

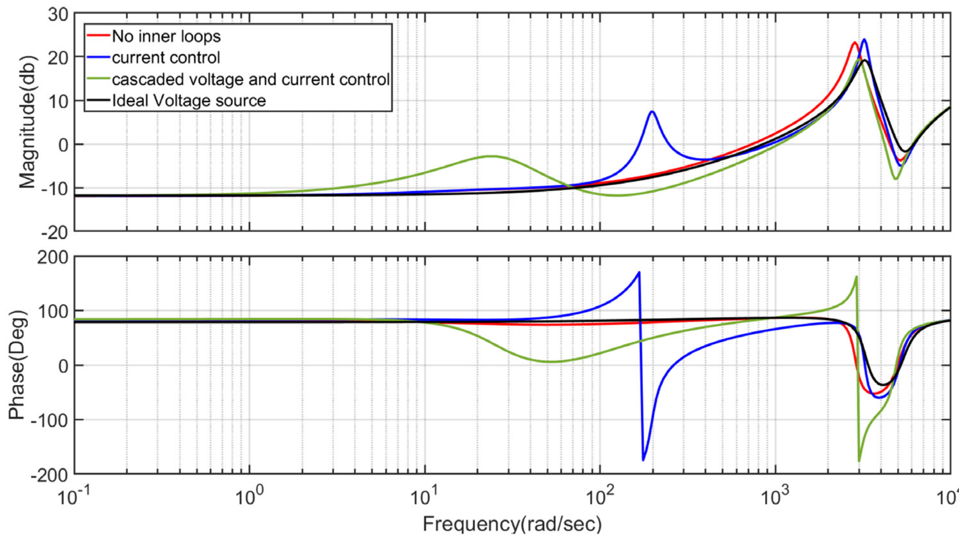

Fig. 15. Dynamic impedance of the GFC's and of the ideal voltage source and impedance.

has the highest deviation from the impedance of the ideal voltage source. The slow dynamics of cascaded control are reflected in the outer impedance, and the output impedance shape follows the ideal impedance only in the low-frequency range. The GFC with no inner loop follows the ideal impedance closely, and the slight difference is due to sampling and PWM delay. The GFC's impedance with only current control is significantly closer to the ideal impedance for a more extended frequency range than the GFC cascaded control.

One key conclusion drawn from the impedance plot is that a virtual impedance-based current limiting scheme that provides a larger transient stability margin Paquette and Divan (2014) lacks a fast response speed to protect the converter sufficiently for a GFC with cascaded control (Qoria et al., 2020). The limitation is even more prominent in large power converters, where the low switching frequency prohibits a high control bandwidth. On the other hand, the virtual impedance method could be sufficiently fast to ensure proper protection for both GFC with only current control and no inner loop case. The implications of the difference in output impedance during transients also have to be carefully studied.

5.3. Passivity analysis of the GFC's impedances

In this section, the dynamic impedance ($Z_{pp}(jw)$) of the three GFC's including the outer loops are analysed in the frequency range of 5 Hz–1 kHz for passivity check.

However, just like an SG, a VSC can never be made entirely passive at all the frequency range (ENTSO-E, 2019). SGs are nonpassive only in the low-frequency range due to slow control and dynamics. Therefore the conventional power system composed mainly of SG-based generation had low-frequency instabilities predominantly (Kundur, 1994). However, the impedance range of nonpassive operation could span a wide bandwidth depending on the control system implemented for VSC. Therefore, the national grid specification of enforcing a passive impedance behaviour in the frequency range of 5 Hz–1 kHz (National Grid ESO, 0000) for GFCs can reduce the negative interactions between the converters and limit the interaction with the network to a low-frequency range. Furthermore, this also comes with the added benefit of the ease of modelling and analysing large systems.

The real part of the modified positive sequence impedance is shown in Fig. 16. It can be seen from both the figures that the GFC without any inner loop behaves as a passive impedance in the frequency of interest, as it does not have a non negative real part. Whereas the $Z_{pp}(jw)$ for both GFC with current control as well as the GFC with cascaded control has a negative real part in the frequency range of 10–15 Hz and 300–600 Hz, respectively, for the designed control parameters. However, when the time constant of the current control is increased to 1 ms for a 10 kHz switched converter, there is no negative resistance region in the output impedance of the GFC. This implies that the presence of an inner loop in low switching frequency converters, as is the case with high power converters, could result in unstable oscillations. The result is similar to the results derived from impedance-based passivity analysis conducted on PLL-based VSC. For instance, Wen et al. (2015) and Harnefors et al. (2015) reported that the current control and feed-forward filters, along with the PLL, also contribute to VSC's nonpassive behaviour. Therefore, merely eliminating the PLL alone is not enough to ensure the converter impedance behaves passively, as it is demonstrated in Fig. 16.

Several past research discusses increasing the range of passivity of power converter impedances, Harnefors et al. (2007), Agbemuko et al. (2020) and Wu and Wang (2020) discuss design techniques and controls for increasing the passivity behaviour of VSC with LCL filter and current control. Similarly, Liao et al. (2020) also discusses the methods for ensuring passivity until the Nyquist frequency range ($0-fs/2$)for cascaded voltage-controlled converters. In conclusion, to this section, it can be said that the requirement of GFC behaving as a voltage source behind an impedance in the frequency range of interest is satisfied for GFC without inner loops. In contrast, it is not straightforward for GFC's with an inner loop to ensure passivity. Furthermore, as the converter is rated for high power, the switching frequency reduces, thus aggravating the stability issues due to the nonpassive behaviour of power converter impedances.

5.4. Impact of inner loop on electromechanical mode

The future power system will be composed of a mix of SG and VSC; hence it is important to study the interaction between GFC and SG. For SG, the damping is realized through damper windings and is typically low, whereas the damping effect for GFC can be easily programmed and may be constrained only by the size of the dc energy storage. Consequently, it is essential to ensure that the inner loops do not affect the electromechanical mode adversely. Such a study should be conducted in a test system

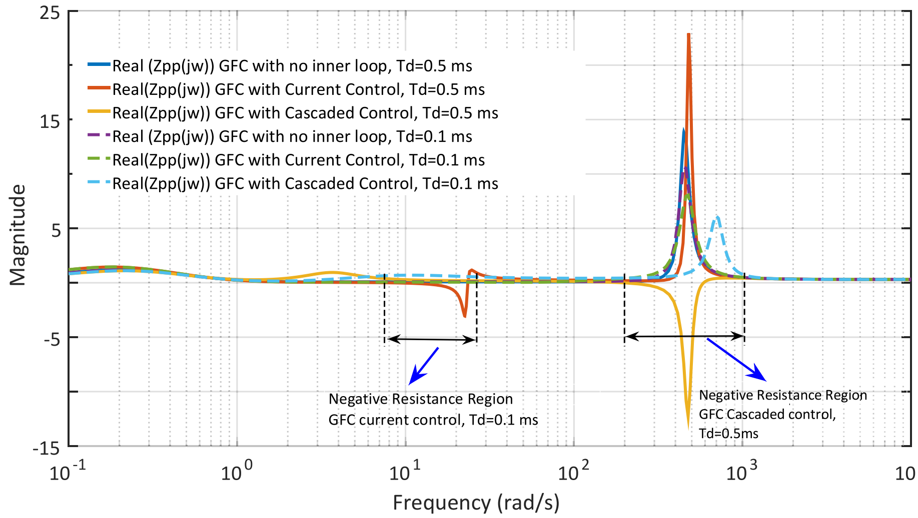

Fig. 16. Real part of the dynamic impedance of the three type of GFC's considered.

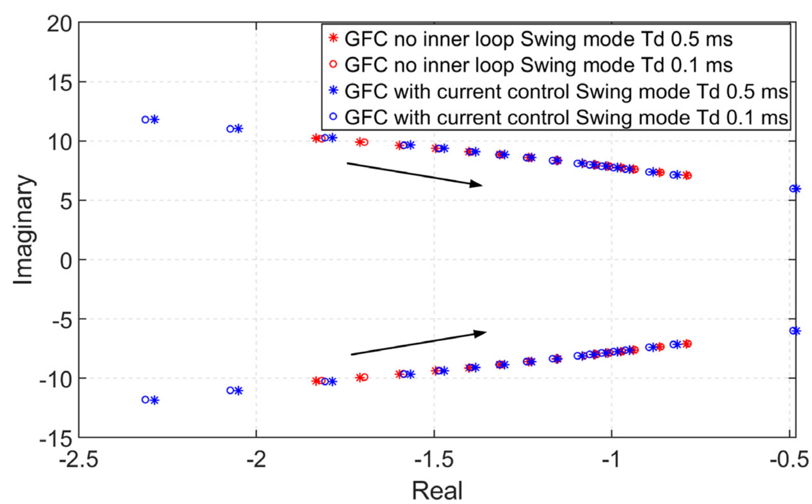

Fig. 17. Trajectory of swing mode of GFC with no inner loop and GFC with current control by simultaneously increasing transmission line impedance's (Z_{TL1}, Z_{TL2}) from 0.01 to 0.5 pu.

consisting of both SG and GFC. Most recent publications (Du et al., 2019; Qu et al., 2020; Li et al., 2020) that investigated GFC with cascaded inner loop did not consider a SG in the studies. Therefore, the local electromechanical oscillation, typically in the frequency of 0.7–2 Hz, is not present in any of these studies. Thus the impact of inner loops on the electromechanical model of SG has not been evaluated. Furthermore, Du et al. (2019) and Li et al. (2020) has no inertia programmed in control; hence an oscillatory mode arising due to virtual inertia is absent.

In this section, a small-signal analysis is carried to evaluate the difference in impact on the electromechanical mode by the three considered GFC's. First, an eigenanalysis is conducted on the derived small-signal model, and the electromechanical modes are identified from the participation factors. Major participants of the swing modes are the SG's rotor speed and active power control loop of the GFC's. In the case of SG, the swing mode moves towards RHP when the grid strength is reduced (Kundur, 1994), and one would expect similar behaviour with the GFC. However, unlike an SG where additional damping has to be provided by indirect means such as power system stabilizers, the GFC can be damped using control parameters.

The trajectory of swing mode of GFC with no inner loop and GFC with current control, by increasing transmission line impedance's (Z_{TL1}, Z_{TL2}) from 0.01 to 0.5 pu is shown in Fig. 17, the case is repeated for GFC switching at 2 kHz and 10 kHz. Compared to GFC without inner loop GFC, the swing modes in GFC with current control are slightly more sensitive to change in grid impedance. However, GFC with current control can provide slightly higher damping in low grid impedance scenarios, but the differences in the trajectory and position of the eigenvalues are not significantly different from each other. It can also be seen that the change in the switching frequency hardly affects the swing modes in both the GFC with current control and GFC with no inner loop. The electromechanical mode in both cases moves to the right as the grid impedance is increased; however, it is quite possible to ensure sufficient damping even at very low grid strength. Compared to GFC without inner loop GFC, swing modes in the case of GFC with current control are slightly more sensitive to change in grid impedances. However, the differences in the trajectory and position of the eigenvalues are not significantly different from each other. It can also be seen that the change in PWM delay hardly affects the swing modes in both the GFC with current control and GFC with no inner loop. From these studies, it can be observed that the presence of an current control alone in GFC with current control does not negatively impact the damping of the electromechanical mode.

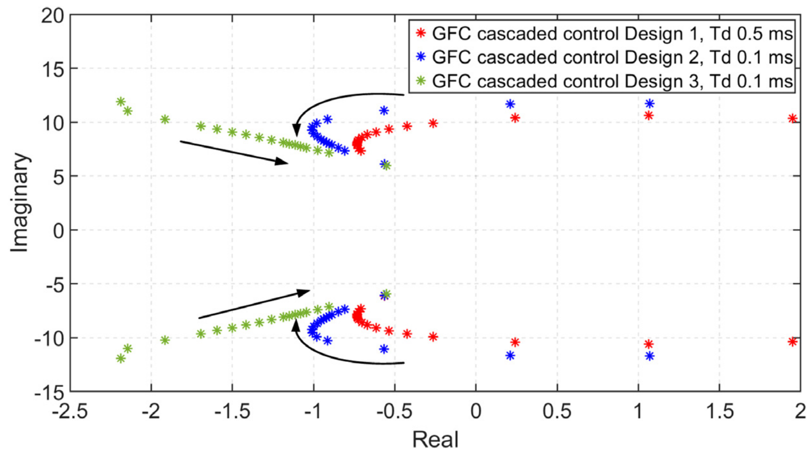

Fig. 18. Trajectory of swing mode of GFC with cascaded inner loop with simultaneously increasing transmission line impedance's (Z_{TL1}, Z_{TL2}) from 0.01 to 0.5 pu for control designs specified in Table 5.

The swing modes of GFC with cascaded inner control by increasing transmission line impedance (Z_{TL1}, Z_{TL2}) from 0.01 to 0.5 pu for all the three control design objectives is shown in Fig. 18. The results of the Eigen trajectory design one and two are shown in Table 5, which are moving left (towards stabler region) initially as the transmission line impedances (Z_{TL1}, Z_{TL2}) are increased before shifting the trajectory back towards RHP. On the other hand, the eigenvalues consistently move towards RHP as the network impedance increases when design parameters of the GFC correspond to design 3 in Table 5. This trajectory is similar to how electromechanical mode would move, as in the case of the other two GFCs or an SG. Furthermore, electromechanical eigenvalues with designs 1 and 2 are always underdamped compared to the electromechanical eigenvalue results with GFC with no inner loop and GFC with current control inner loop at similar grid strength. On the other hand, GFC with cascaded control provided equivalent damping to the electromechanical mode similar to the GFC with no inner loop and GFC with current control inner loop with the third set of control parameters.

The Du et al. (2019), Qu et al. (2020) and Li et al. (2020), concludes that an increase in grid impedance is better for the stability of the GFC with cascaded voltage control. Although the test system and outer loop parameters are different with Du et al. (2019), Qu et al. (2020) and Li et al. (2020), the eigen analysis presented in this paper shows that such a conclusion is not unconditionally true and can depend on the system considered, control design, power rating, and structure of the cascaded voltage control.

6. Time domain simulation study

The focus on the time-domain analysis presented in this section is to verify the conclusions drawn in small-signal analysis and verify if the response from all the three GFC types is similar to a voltage source. It is concluded in the small-signal analysis that the GFC types with inner loops for MW level converter could be nonpassive in certain frequency ranges. Also, it is concluded that the GFC with cascaded control could negatively impact the electromechanical damping when system strength improves. The time-domain simulation results presented validate this conclusion.

6.1. Response of the GFC's during voltage phase and magnitude change events

This section assess the response of the considered GFC's for voltage change events. It has to be noted that for large faults the control realizations require careful consideration of antiwindup schemes for the control loops (Qoria et al., 2020) and an assessment of transient stability (Kkuni and Yang, 2021). For the sake of brevity, this paper only considers GFC with an implementation of the current limits and does not include additional control logics for anti windup and increasing transient stability.

The grid forming capability of the GFC is evaluated against a step change in infinite bus voltage and step change in angle of the infinite bus without the current limiting logic. The GFC POC bus is connected to the infinite bus through a 0.1 p.u reactance. The net steady state impedance between the infinite bus and the voltage source representing GFC will include the physical network impedance of 0.2 p.u and the impedance of 0.15 p.u of GFC internal impedance. It has to be noted that the GFC internal impedance is emulated using virtual impedance as in the case of GFC with inner loop, or adjusted with filter impedance to get total of 0.15 p.u for GFC with no inner loops. The output response of a voltage source behind an impedance against a grid event depends on the total impedance and the magnitude of the voltage, which in this case is similar for all the three converter in steady state. Since the GFC's implemented have similar internal impedance, the responses are also expected to be same.

For a dip in infinite bus voltage to 0.5 p.u, the considered GFC's with inactive current limitation algorithm have similar responses from the three GFC's considered in steady-state as seen in Fig. 20. However, the GFC with a cascaded inner loop has a larger than expected spike immediately after the dip in voltage compared to the other two. Such spike can be attributed to the cascaded loop's slow dynamics, resulting in an emulated impedance that is relatively slow and presents a varying impedance than a constant impedance. The impact of this slow dynamics of the virtual impedance for cascaded control is also seen in response to the phase jump of the infinite bus voltage, as seen in Fig. 21. The slow varying impedance is an undesirable characteristic as it can trigger the current limit and presents a problem in dynamic power-sharing under parallel connection of voltage sources.

The performance of the GFC's when subjected to a large dip in infinite bus voltage to 0.4 pu with current limit logic activated is shown in Fig. 22. As expected, the impedance-based current limit implemented on GFC with cascaded inner loops has the highest peak current and is above the 1.2 pu, which is chosen overload rating. The GFC with inner current control has the fastest current limit action, with the peak current not exceeding the set nominal peak current value. However the key take away is that it is possible to effectively limit the current for all the three control strategies as also demonstrated from the results for the fault simulation with a voltage dip to 0.4 pu for 200 ms in Fig. 23.

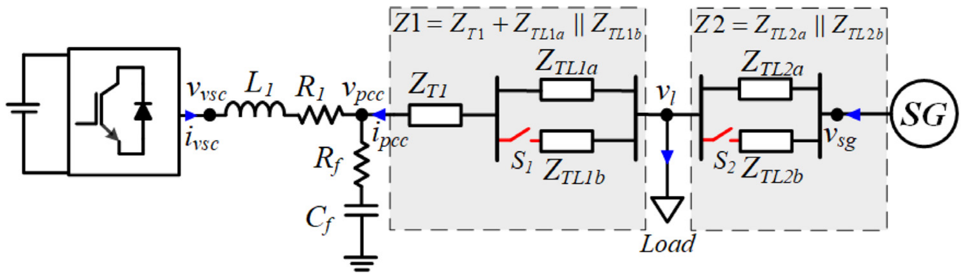

Fig. 19. The test system to evaluate the implication of different impedance behaviour and robustness of the three GFC's against a network impedance change.

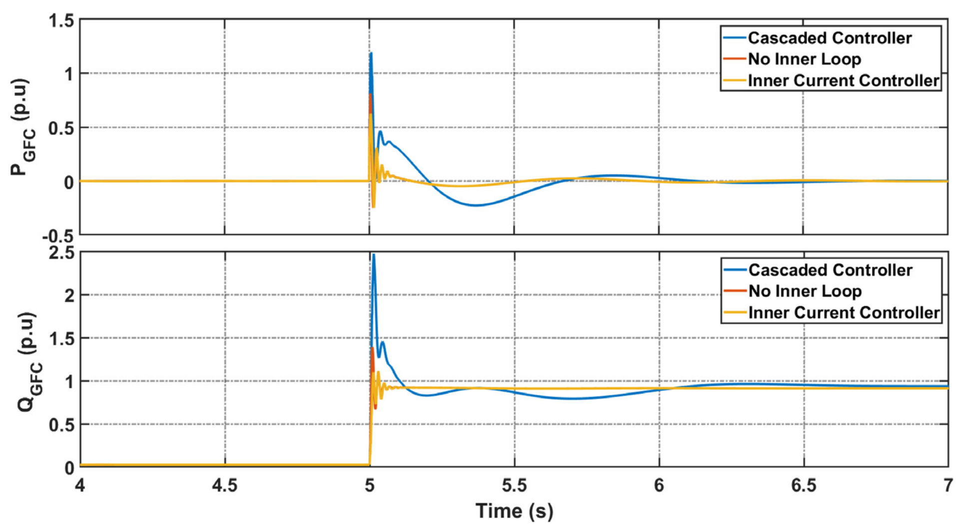

Fig. 20. GFC active power and reactive power output in response for an infinite bus voltage dip to 0.5 p.u, with inactive current limitation algorithm.

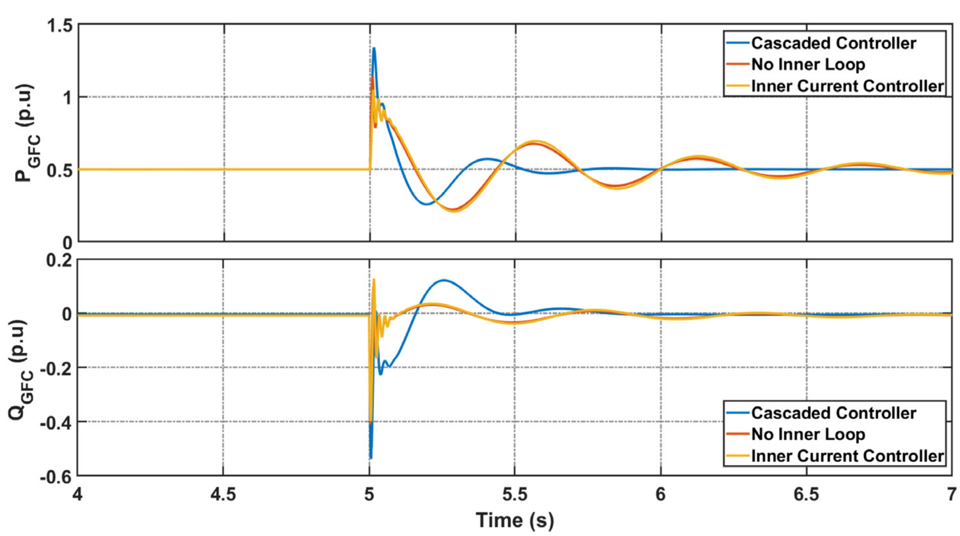

Fig. 21. GFC active power and reactive power output in response for a infinite bus angle jump of 10 degree, with inactive current limitation algorithm.

6.2. Case study

A time domain Case study to evaluate the implication of different impedance behaviour and robustness of the three GFC's against a network impedance change are conducted. The GFC with time delay corresponding to PWM frequency of 2 kHz is chosen for the study. The time domain study is closely aligned with the small signal analysis presented in Section 5. A test system as shown in Fig. 19 is implemented in MATLAB/SIMULINK. The impedance Z1 is the net impedance between PCC bus and load bus, and Z2 is the net impedance between load and SG bus. For the first case, the three GFC's are evaluated against an increase in network impedance change event. During pre-network impedance change event, the switch S2 is off and S1 is on, ensuring both Z1 and Z2 to be 0.2 pu. Also, both the SG and the GFC's are sharing 1 pu load equally between the them. Switch S1 is opened at 5 s, increasing impedance between the PCC bus and the load bus (Z1) to 0.6 pu. The test case is repeated for systems with all the three GFC's. As seen in Fig. 24, the GFC without inner loop behaves as voltage source behind an impedance and settling

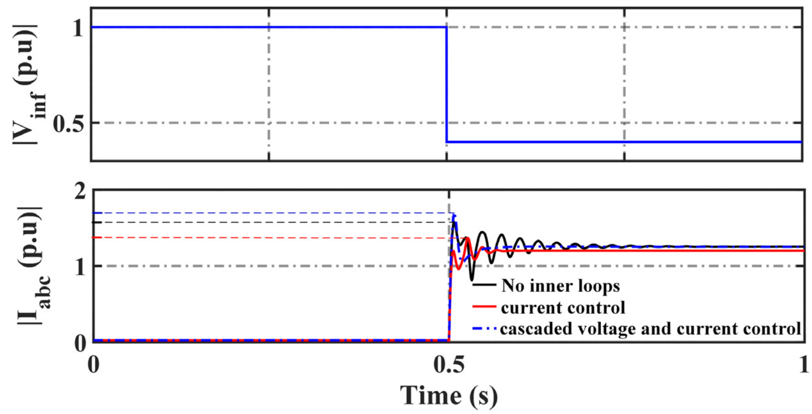

Fig. 22. The output current magnitude of GFC's for an infinite bus voltage dip to 0.5 p.u, with active current limitation algorithm.

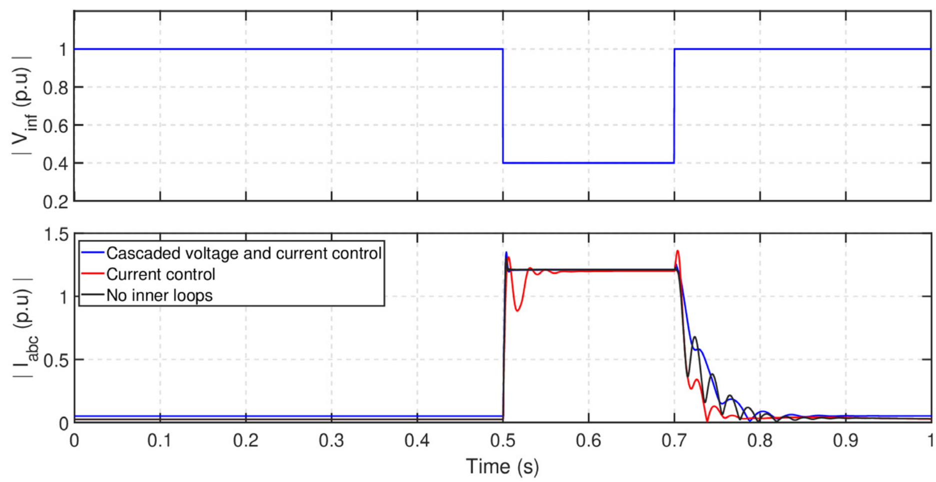

Fig. 23. The output current magnitude of GFC's for an fault case simulation with voltage dip to 0.4 p.u, and clearing after 200 ms, with active current limitation algorithm.

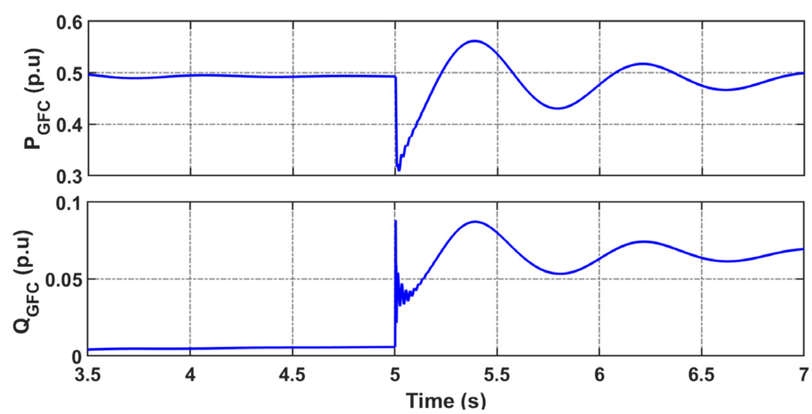

Fig. 24. Active and reactive power response of the GFC with no inner loop under network impedance Z1 increase from 0.15 pu to 0.6 pu.

to steady state as soon as the swing mode are damped out. The results align with that of Section 5, which predicted the GFC with no inner loop is passive and swing modes are also damped for all possible network impedance combinations. On the other hand, both GFC with current control inner loop and GFC with cascaded control become unstable with an increase in network impedance, as depicted in Fig. 26 and Fig. 25, respectively. These instabilities result in oscillation frequencies that fall outside the passive frequency range of their respective impedances.

The investigating on swing modes and network impedance revealed that the high power GFC with cascaded control, switching at low frequency could have underdamped or undamped electromechanical mode when the network impedances are reduced. Such a characteristics is unlike an SG or the other configuration of GFC's and is unique to GFC with cascaded control. The simulations are conducted with GFC cascaded control with the three design shown in Table 5 with the network impedance Z1 and Z2 decreased from 0.2 pu to 0.1 pu at 15 s. The results are depicted in Fig. 27. It can be seen that for design one with lower switching

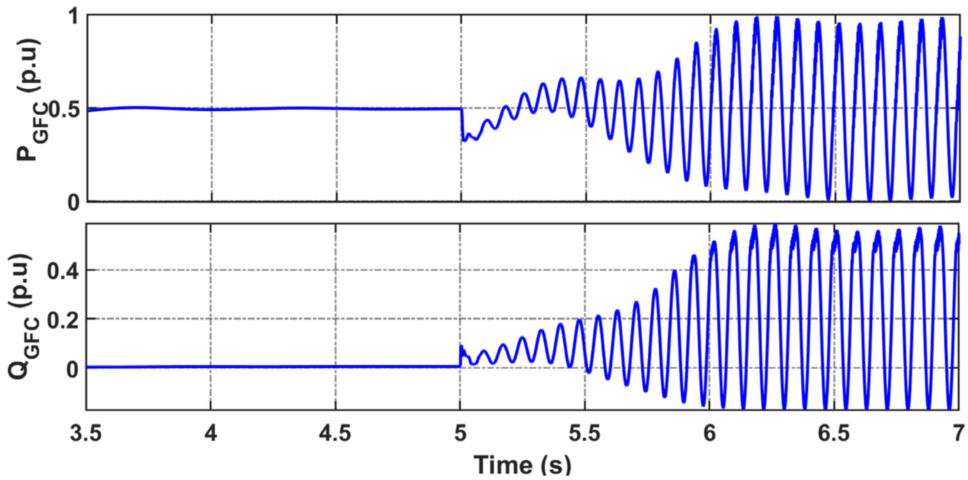

Fig. 25. Active and reactive power response of the GFC with current control inner loop under network impedance Z1 increase from 0.15 pu to 0.6 pu.

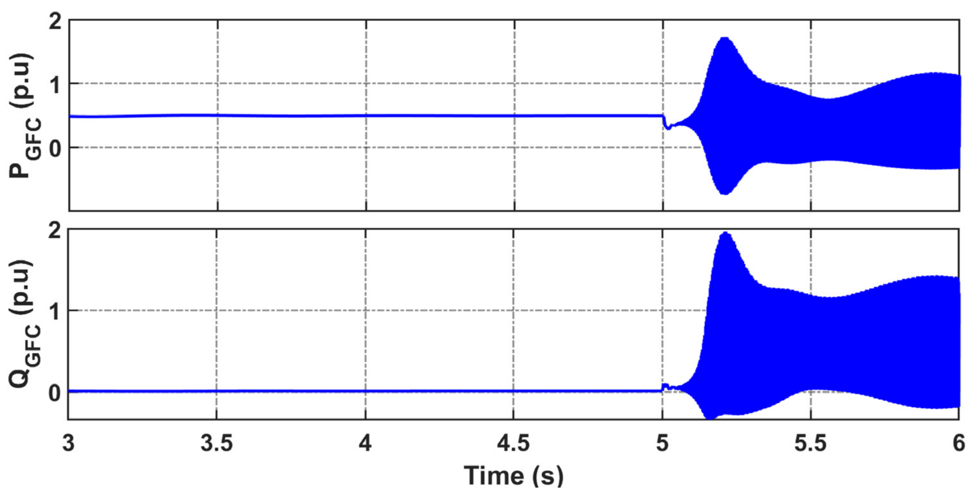

Fig. 26. Active and reactive power response of the GFC cascaded inner loop under network impedance Z1 increase from 0.15 pu to 0.6 pu.

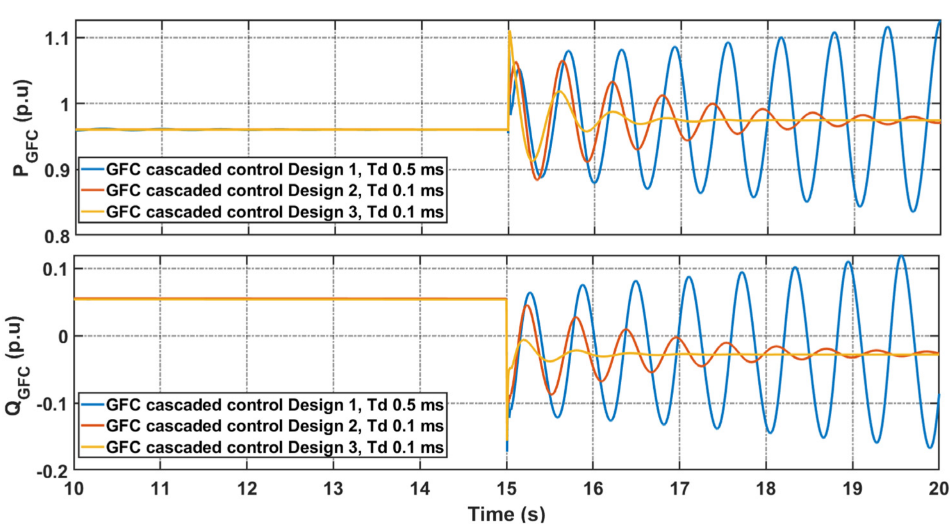

Fig. 27. Active and reactive power time domain response of the GFC with cascaded control when network impedance Z1 and Z2 decreased from 0.2 pu to 0.1 pu.

frequency the swing modes get undamped at 15 s, whereas, if the switching frequency was higher as in the case of design 2 and 3 the electromechanical mode is still stable.

The behaviour of the GFC for a 3-phase fault case is shown in Fig. 28, which demonstrates a fast fault current contribution from all the three cases, with cascaded inner loop GFC a larger

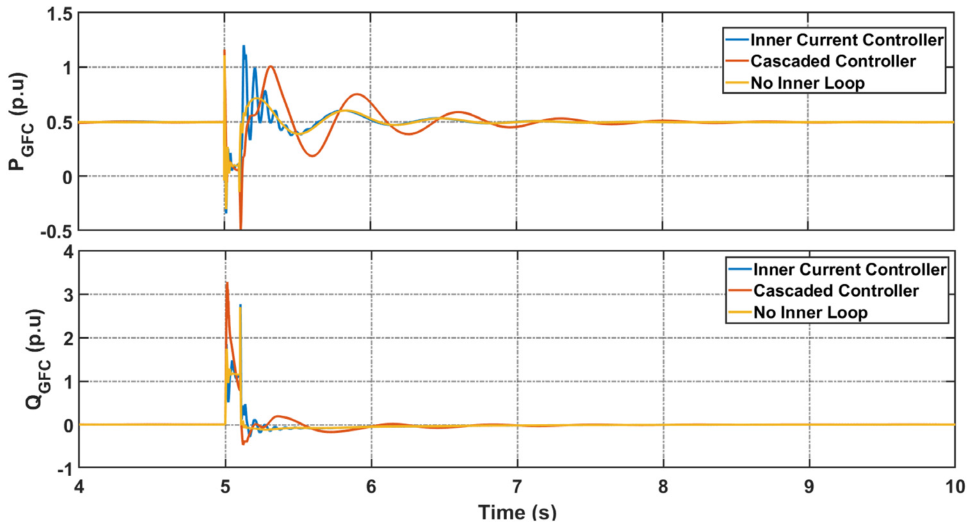

Fig. 28. GFC active power and reactive power output in response for a 3L-G fault.

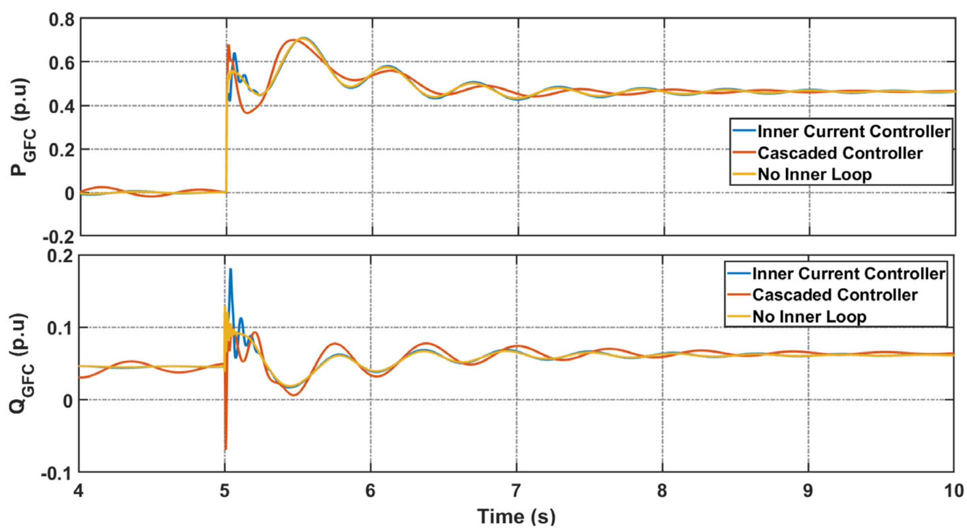

Fig. 29. GFC active power and reactive power output in response for a 0.5 p.u load switching.

current contribution in the beginning of the fault can be seen due to the slow dynamics of the virtual impedance. One of the main advantage of a synchronous machine, being a voltage source is that it can contribute to load sharing instantly without relying on control or measurements. The results for a 0.5 p.u load turn on and off when the net impedance between PCC and load is 0.15 p.u is shown in Figs. 29 and 30. The response shows that all the three GFC have voltage source characteristics as the load is shared instantly by the GFC's. On closer examination it can be seen that power shared at the load switching instant is slightly higher for cascaded inner loop GFC case due to slow dynamics of the virtual impedance.

7. Summary

Assessing the dynamic impedance of the three GFC's derived from the small-signal shows that it is challenging to ensure a passive impedance behaviour in a broad frequency range for GFC with an inner loop. This is particularly true for high power GFC's with low switching frequency because of the PWM delay. Because of this, unstable oscillations may arise for a system composed of GFCs with inner loops under weak grid conditions.

Furthermore, time domain studies performed showed that the GFC configuration with the inner current control and no inner loop could respond similar as a voltage source under a strong grid scenario. Whereas, for the GFC with a cascaded inner loop, the impedance is found to be slow-acting and only effective in very low frequency range because of the loop delays. This slow acting virtual impedance of the cascaded GFC results in higher than expected instantaneous active power and reactive power for a grid event, which may trigger unexpected overcurrent protection of the semiconductor devices. Moreover, this slow-acting virtual impedance is seen as a slowly changing time-varying impedance in the GFC's terminal characteristics with cascaded control, causing problems in dynamic reactive power-sharing. Furthermore, the slow-acting virtual impedance can also limit the application of virtual impedance based current limiting method.

Additionally, a study on the electromechanical oscillation mode of the SG was conducted with the three GFC configurations. It was found that the impact of PWM delays for GFC configuration with no inner loop or only inner current controller is marginal. The damping of the electromechanical mode for GFC configuration with no inner loop or only inner current controller is better than GFC with cascaded control at all network strengths. The electromechanical oscillation mode is sensitive for the GFC with

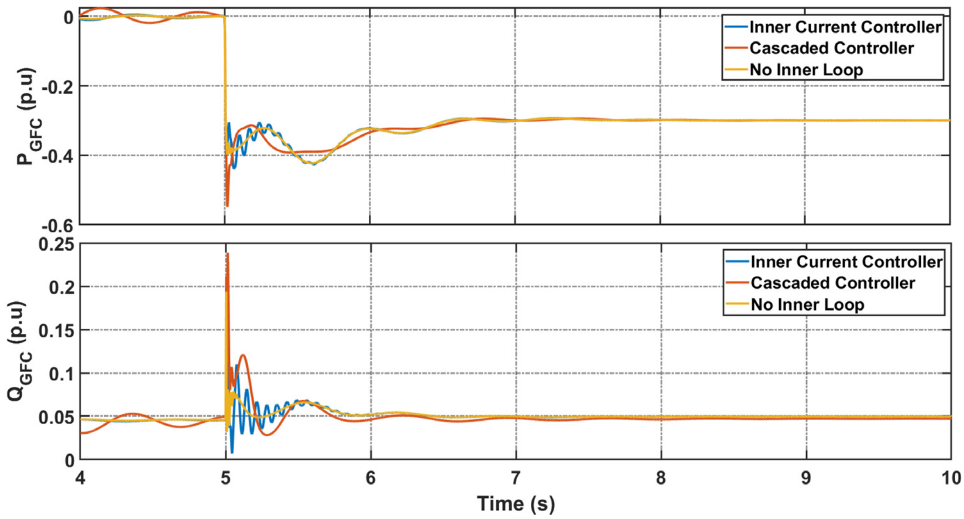

Fig. 30. GFC active power and reactive power output in response for a 0.5 p.u load disconnection.

Table 6
Summary of GFC comparisons.

	GFC with no inner loop	GFC with inner current control	GFC with cascaded voltage control
Passivity Beyond outer control Bandwidth	Passive	Possibility for not passive at frequency determined by feed forward filter and control bandwidth	Possibility for not Passive around resonant frequency range
Constraint on network impedance	No constraint	Upper limit in non passive region	Both upper and lower limit
Dynamic power-sharing	Behaves like a voltage source behind a fixed reactance	Behaves like a voltage source behind a fixed reactance	Behaves like a voltage source behind a time varying reactance due to slow acting virtual impedance
Virtual impedance current limiting	Possible	Current overshoot is tightly controlled	Slow action due to slow acting virtual impedance
Electro-mechanical eigen value	No negative impact on damping	No negative impact on damping	Negative impact on damping, depends on control design

cascaded control. This type of control can be unstable with low network impedance unlike an SG or the other configurations of GFC. The electromechanical oscillation mode can move towards a more stable region as the network impedance is increased. Consequently, GFC with cascaded control could have both an upper bound on the network impedance due to passivity-related high-frequency oscillations and a lower bound for network impedance to ensure sufficient damping for critical electromechanical modes.

Furthermore, this paper shows that weakening of the damping on electromechanical modes with an increase in grid strength is control and switching frequency dependent, and reverse could also be true for a different control design and switching frequency. With another control design objective and higher switching frequency, one can achieve similar damping for electromechanical mode with the GFC with cascaded control as that of the GFC with no inner loop. The key differences among the considered GFCs are summarized in Table 6.

8. Conclusion

This work provides a critical review on the inner loop realization of GFCs and the impacts of different methods on the ability of GFCs to behave like a voltage source behind an impedance characteristic for fundamental frequency. The GFC is also expected to be a sink for harmonics and unbalances (ENTSO-E, 2019). Only GFC with no inner loop and programmed inertia can present a natural sink to harmonics, inter-harmonics, and unbalance, within the hardware capability without making any changes to the control structures. The GFC with inner loops would require additional control loops to sink for the harmonics and unbalance similar to a grid following converter (Remus Teodorescu and Rodríguez, 2011). On the other hand, with additional parallel loops, the GFC with inner loops can respond selectively to the harmonics or unbalances, which could be beneficial for the system. In this case, the open question would be on standardizing the harmonic contributions required from GFC's.

To address the challenge of adverse interactions in the higher frequency range of GFCs, one potential research direction is the development of accurate RMS models. However, this presents a significant challenge as the dynamics of GFCs cannot always be adequately captured by traditional RMS models. To improve the accuracy of the models, it is essential to set constraints on the bandwidth and stability margin of GFC controls. Moreover, these models should also be validated against EMT models through system simulations. Currently, there is a lack of a defined workflow and test systems for validating the RMS models of GFCs in the literature.

The GFC synchronization and power control loop are the same. Therefore, unlike the conventional grid following converters which directly controls the active and reactive current setpoints and the option to limit the active or reactive power without affecting voltage-based synchronization, implementing the power or current limiters for GFC is challenging. The current and power limit could be triggered during faults or from overload scenarios arising from changing system frequencies. There is a necessity for coordination between the power control loop and the current limiter. The challenge of current limiting control is even greater for GFC with no inner loop. It has been implemented by virtual impedance with power loop frozen (Yu et al., 2015), by switching the grid forming control to PLL-based grid following control (Zhang, 2010), by adaptive change of the droop parameters (Großand Dörfler, 2019), or by employing voltage limitation for current limitations (Chen et al., 2020a). However, the focus of the studies has been limited to either current limiting during a short circuit or overload. In general, the current and power limiter needs to be robust against both overload and fault cases, and must also be demonstrated in a test system. Furthermore, the GFC impact on frequency stability, back-end system (such as wind turbine, solar PV, or battery), and current limiting functions need to be thoroughly studied. Additionally, impact of virtual impedance based current limiting method on the system strength also requires further studies to understand the impact on system stability under different dynamic scenarios.

Declaration of competing interest

The authors declare that they have no known competing financial interests or personal relationships that could have appeared to influence the work reported in this paper.

Data availability

Data will be made available on request

Acknowledgements

The study is funded by Phoenix project, funded by Ofgem under Network Innovation Competition programme, Project Direction ref: SPT/Phoenix / 16 December 2016 (https://www.spenergynetworks.co.uk/pages/phoenix.aspx). Authors would also like to acknowledge Thyge Knueppel from Siemens Gamesa, Jay Ramachandran National Grid, Qiteng Hong and Campbell Booth from University of Strathclyde for their valuable feedbacks during the paper preparations.

References

Agbemuko, Adedotun J., Dominguez-Garcia, Jose Luis, Gomis-Bellmunt, Oriol, Harnefors, Lennart, 2020. Passivity-based analysis and performance enhancement of a vector controlled VSC connected to a weak AC grid. IEEE Trans. Power Deliv..

Cheema, Khalid Mehmood, 2020. A comprehensive review of virtual synchronous generator. Int. J. Electr. Power Energy Syst. 120, 106006.

Chen, Junru, Prystupczuk, Federico, O'Donnell, Terence, 2020a. Use of voltage limits for current limitations in grid-forming converters. CSEE J. Power Energy Syst. 6 (2), 259–269.

Chen, Meng, Zhou, Dao, Blaabjerg, Frede, 2020b. Modelling, implementation, and assessment of virtual synchronous generator in power systems. J. Mod. Power Syst. Clean Energy 8 (3), 399–411.

Collados-Rodriguez, Carlos, Cheah-Mane, Marc, Prieto-Araujo, Eduardo, Gomis-Bellmunt, Oriol, 2019. Stability analysis of systems with high VSC penetration: Where is the limit? IEEE Trans. Power Deliv..

Cunha, Vinicius C., Kim, Taehyung, Barry, Nicholas, Siratarnsophon, Piyapath, Santoso, Surya, Freitas, Walmir, Ramasubramanian, Deepak, Dugan, Roger C., 2021. Generalized formulation of steady-state equivalent circuit models of grid-forming inverters. IEEE Open Access J. Power Energy 8, 352–364.

Denis, Guillaume, Prevost, Thibault, Debry, Marie-Sophie, Xavier, Florent, Guillaud, Xavier, Menze, Andreas, 2018. The migrate project: The challenges of operating a transmission grid with only inverter-based generation. A grid-forming control improvement with transient current-limiting control. IET Renew. Power Gener. 12 (5), 523–529.

Du, Wei, Chen, Zhe, Schneider, Kevin P., Lasseter, Robert H., Nandanoori, Sai Pushpak, Tuffner, Francis K., Kundu, Soumya, 2019. A comparative study of two widely used grid-forming droop controls on microgrid small-signal stability. IEEE J. Emerg. Sel. Top. Power Electron. 8 (2), 963–975.

ELectranet, 2021. ESCRI-SA Battery Energy Storage Project Operational Report #3. Technical Report.

ENTSO-E, 2019. High penetration of power electronic interfaced power sources and the potential contribution of grid forming converters. p. 32.

ENTSO-E guidance document for national implementation for network codes on grid connection, 2017. Fault Current Contribution from PPMS & HVDC. Technical Report, Draft of Expert Group FFCI.

Eriksson, Robert, Modig, Niklas, Elkington, Katherine, 2017. Synthetic inertia versus fast frequency response: A definition. IET Renew. Power Gener. 12 (5), 507–514.

Groß, Dominic, Dörfler, Florian, 2019. Projected grid-forming control for current-limiting of power converters. In: 2019 57th Annual Allerton Conference on Communication, Control, and Computing. Allerton, IEEE, pp. 326–333.

Harnefors, Lennart, Bongiorno, Massimo, Lundberg, Stefan, 2007. Input-admittance calculation and shaping for controlled voltage-source converters. IEEE Trans. Ind. Electron. 54 (6), 3323–3334.

Harnefors, Lennart, Wang, Xiongfei, Yepes, Alejandro G., Blaabjerg, Frede, 2015. Passivity-based stability assessment of grid-connected VSCs—An overview. IEEE J. Emerg. Sel. Top. Power Electron. 4 (1), 116–125.

Homan, Samuel, Mac Dowell, Niall, Brown, Solomon, 2021. Grid frequency volatility in future low inertia scenarios: Challenges and mitigation options. Appl. Energy 290, 116723.

Ierna, Richard, Dyśko, Adam, Booth, Campbell, 2019. Enhanced virtual synchronous machine (VSM) control algorithm for hybrid grid forming converters. 18th Wind Integr. Work..

Ierna, Richard, Zhu, Jiebei, Roscoe, Andrew J., Yu, Mengran, Dysko, Adam, Booth, Campbell D., Urdal, Helge, 2016. Effects of VSM convertor control on penetration limits of non-synchronous generation in the GB power system. In: 15th Wind Integration Workshop.

Inertia2020 Working Group, 2020. Technical requirements for fast frequency reserve provision in the Nordic Synchronous Area – external document. Technical Report, ENTSO-E.

Jia, Jundi, Yang, Guangya, Nielsen, Arne Hejde, Muljadi, Eduard, Weinreich-Jensen, Peter, Gevorgian, Vahan, 2018a. Synchronous condenser allocation for improving system short circuit ratio. In: 2018 5th International Conference on Electric Power and Energy Conversion Systems. EPECS, IEEE, pp. 1–5.

Jia, Jundi, Yang, Guangya, Nielsen, Arne Hejde, Rønne-Hansen, Peter, 2018b. Impact of VSC control strategies and incorporation of synchronous condensers on distance protection under unbalanced faults. IEEE Trans. Ind. Electron. 66 (2), 1108–1118.

Johnson, Samuel C., Rhodes, Joshua D., Webber, Michael E., 2020. Understanding the impact of non-synchronous wind and solar generation on grid stability and identifying mitigation pathways. Appl. Energy 262, 114492.

Kkuni, Kanakesh Vatta, Ghosh, Sujay, Yang, Guangya, Booth, Campbell, 2019. Modelling and passivity analysis of VSC output impedance under SRF and alpha-beta control frames. In: IECON 2019-45th Annual Conference of the IEEE Industrial Electronics Society, Vol. 1. IEEE, pp. 1856–1861.

Kkuni, Kanakesh Vatta, Yang, Guangya, 2021. Effects of current limit for grid forming converters on transient stability: analysis and solution.

Kundur, Prabha, 1994. Power System Stability and Control. McGraw-Hill Education.

Lasseter, Robert H., Chen, Zhe, Pattabiraman, Dinesh, 2019. Grid-forming inverters: A critical asset for the power grid. IEEE J. Emerg. Sel. Top. Power Electron. 8 (2), 925–935.

Li, Xin, Chen, Guozhu, Ali, Muhammad Saqib, 2019. Improved virtual synchronous generator with transient damping link and its seamless transfer control for cascaded H-bridge multilevel converter-based energy storage system. IET Electr. Power Appl. 13 (10), 1535–1543.

Li, Chuanyue, Liang, Jun, Cipcigan, Liana M, Ming, Wenlong, Colas, Frederic, Guillaud, Xavier, 2020. DQ impedance stability analysis for the power-controlled grid-connected inverter. IEEE Trans. Energy Convers. 35 (4), 1762–1771.

Liao, Yicheng, Wang, Xiongfei, Blaabjerg, Frede, 2020. Passivity-based analysis and design of linear voltage controllers for voltage-source converters. IEEE Open J. Ind. Electron. Soc. 1, 114–126.

Liu, Jia, Miura, Yushi, Ise, Toshifumi, 2015. Comparison of dynamic characteristics between virtual synchronous generator and droop control in inverter-based distributed generators. IEEE Trans. Power Electron. 31 (5), 3600–3611.

Liu, Teng, Wang, Xiongfei, Liu, Fangcheng, Xin, Kai, Liu, Yunfeng, 2021. A current limiting method for single-loop voltage-magnitude controlled grid-forming converters during symmetrical faults. IEEE Trans. Power Electron. 37 (4), 4751–4763.

Ma, Yiwei, Cao, Wenchao, Yang, Liu, Wang, Fei, Tolbert, Leon M, 2017. Virtual synchronous generator control of full converter wind turbines with short-term energy storage. IEEE Trans. Ind. Electron. 64 (11), 8821–8831.

Markovic, Uros, Stanojev, Ognjen, Vrettos, Evangelos, Aristidou, Petros, Hug, Gabriela, 2019. Understanding Stability of Low-Inertia Systems. engrXiv.

Marrazi, Emanuel, Yang, Guangya, Weinreich-Jensen, Peter, 2018. Allocation of synchronous condensers for restoration of system short-circuit power. J. Mod. Power Syst. Clean Energy 6 (1), 17–26.

Milano, Federico, Dörfler, Florian, Hug, Gabriela, Hill, David J., Verbič, Gregor, 2018. Foundations and challenges of low-inertia systems. In: 2018 Power Systems Computation Conference. PSCC, IEEE, pp. 1–25.

Natarajan, Vivek, Weiss, George, 2017. Synchronverters with better stability due to virtual inductors, virtual capacitors, and anti-windup. IEEE Trans. Ind. Electron. 64 (7), 5994–6004.
National Grid Electricity System Operator, 2020. The Grid Code (UK), (5). pp. 0–1014.
National Grid ESO, 0000. Stability Pathfinder – Oct 2019, Draft Grid Code – Grid Forming and Request for Information Feedback, Technical Report.
National Grid ESO, 0000. System Operability Framework (SOF)-The potential operability benefits of Virtual Synchronous Machines and related technologies, URL https://www.nationalgrideso.com/document/168376/download.
Nationalgrideso, 2021. Operability Strategy Report 2021. Technical Report, Nationalgrideso.
NERC, 2018. Reliability Guideline: BPS-Connected InverterBased Resource Performance. Atlanta, GA.
Nguyen, Ha Thi, Yang, Guangya, Nielsen, Arne Hejde, et al., 2017. Frequency stability enhancement for low inertia systems using synthetic inertia of wind power. In: 2017 IEEE Power & Energy Society General Meeting. IEEE, pp. 1–5.
Nuhic, Mirza, Kkuni, Kanakesh Vatta, Ramachandran, Jay, 2020. Comparative study of hybrid synchronous condenser incorporating battery energy storage system for ancillary service provision. In: Proceedings of the 18th Wind Integration Workshop, Energynautics GmbH.
Paolone, Mario, Gaunt, Trevor, Guillaud, Xavier, Liserre, Marco, Meliopoulos, Sakis, Monti, Antonello, Van Cutsem, Thierry, Vittal, Vijay, Vournas, Costas, 2020. Fundamentals of power systems modelling in the presence of converter-interfaced generation. Electr. Power Syst. Res. 189, 106811.
Paquette, Andrew D., Divan, Deepak M., 2014. Virtual impedance current limiting for inverters in microgrids with synchronous generators. IEEE Trans. Ind. Appl. 51 (2), 1630–1638.
Pattabiraman, Dinesh, Lasseter, R.H., Jahns, T.M., 2018. Comparison of grid following and grid forming control for a high inverter penetration power system. In: 2018 IEEE Power & Energy Society General Meeting. PESGM, IEEE, pp. 1–5.
Poolla, Bala Kameshwar, Groß, Dominic, Dörfler, Florian, 2019. Placement and implementation of grid-forming and grid-following virtual inertia and fast frequency response. IEEE Trans. Power Syst. 34 (4), 3035–3046.
Prevost, Thibault, Denis, Guillaume, 2019. WP3 - Control and Operation of a Grid with 100 % Converter-Based Devices Deliverable 3 . 6: Requirement guidelines for operating a grid with 100% power electronic devices. MIGRATE - Massive Integr. Power Electron. Devices (2019).
Qoria, Taoufik, Gruson, Francois, Colas, Fréderic, Kestelyn, Xavier, Guillaud, Xavier, 2020. Current limiting algorithms and transient stability analysis of grid-forming VSCs. Electr. Power Syst. Res. 189, 106726.
Qu, Zisen, Peng, Jimmy Chih-Hsien, Yang, Huan, Srinivasan, Dipti, 2020. Modeling and analysis of inner controls effects on damping and synchronizing torque components in VSG-controlled converter. IEEE Trans. Energy Convers..
Ratnam, Kamala Sarojini, Palanisamy, K., Yang, Guangya, 2020. Future low-inertia power systems: Requirements, issues, and solutions-A review. Renew. Sustain. Energy Rev. 124, 109773.
Remon, Daniel, Zhang, Weiyi, Luna, Alvaro, Candela, Ignacio, Rodriguez, Pedro, 2017. Grid synchronization of renewable generation systems using synchronous power controllers. In: 2017 IEEE 6th International Conference on Renewable Energy Research and Applications. ICRERA, IEEE, pp. 169–174.
Remus Teodorescu, Marco Liserreand, Rodríguez, Pedro, 2011. Grid Converters for Photovoltaic and Photovoltaic and. pp. 51–56.
Rezkalla, Michel, Zecchino, Antonio, Martinenas, Sergejus, Prostejovsky, Alexander M., Marinelli, Mattia, 2018. Comparison between synthetic inertia and fast frequency containment control based on single phase EVs in a microgrid. Appl. Energy 210, 764–775.
Rodriguez, P., Candela, I., Luna, A., 2013. Control of PV generation systems using the synchronous power controller. In: 2013 IEEE Energy Conversion Congress and Exposition. IEEE, pp. 993–998.
Roscoe, A., Brogan, P., Elliott, D., Knueppel, T., Gutierrez, I., Perez Campion, J.C., Da Silva, R., 2019. Practical experience of operating a grid forming wind park and its response to system events. In: Proceedings of the 18th Wind Integration Workshop, Energynautics GmbH.
Roscoe, Andrew, Knueppel, Thyge, Da Silva, Ricardo, Brogan, Paul, Gutierrez, Isaac, Elliott, Douglas, Campion, Juan-Carlos Perez, 2020. Response of a grid forming wind farm to system events, and the impact of external and internal damping. IET Renew. Power Gener..
Rosso, Roberto, Wang, Xiongfei, Liserre, Marco, Lu, Xiaonan, Engelken, Soenke, 2021. Grid-forming converters: Control approaches, grid-synchronization, and future trends-A review. IEEE Open J. Ind. Appl.
Rygg, Atle, Molinas, Marta, Zhang, Chen, Cai, Xu, 2016. A modified sequence-domain impedance definition and its equivalence to the dq-domain impedance definition for the stability analysis of AC power electronic systems. IEEE J. Emerg. Sel. Top. Power Electron. 4 (4), 1383–1396.
SCAPP, Synchronous Condensers Application in Low Inertia Systems (SCAPP), URL http://www.scapp.dk/home.
Shi, Kai, Chen, Cheng, Sun, Yuxin, Xu, Peifeng, Yang, Yongheng, Blaabjerg, Frede, 2020. Rotor inertia adaptive control and inertia matching strategy based on parallel virtual synchronous generators system. IET Gener. Transm. Distrib. 14 (10), 1854–1861.
SP Energy Networks, Phoenix – system security and synchronous condenser, URL https://www.spenergynetworks.co.uk/pages/phoenix.aspx.
Stojanovic, N., Grcar, M., Sen, S., Ma, J., 2019. Deliverable D1. 1 Report. MIGRATE - Massive Integr. Power Electron. Devices (691800).
Sun, Dawei, Liu, Hui, Gao, Shunan, Wu, Linlin, Song, Peng, Wang, Xiaosheng, 2020. Comparison of different virtual inertia control methods for inverter-based generators. J. Mod. Power Syst. Clean Energy 8 (4), 768–777.
Suntio, Teuvo, Messo, Tuomas, Puukko, Joonas, 2017. Power Electronic Converters: Dynamics and Control in Conventional and Renewable Energy Applications. John Wiley & Sons.
Tamrakar, Ujjwol, Shrestha, Dipesh, Maharjan, Manisha, Bhattarai, Bishnu P., Hansen, Timothy M., Tonkoski, Reinaldo, 2017. Virtual inertia: Current trends and future directions. Appl. Sci. 7 (7), 654.
Taul, Mads Graungaard, Wang, Xiongfei, Davari, Pooya, Blaabjerg, Frede, 2019. Current limiting control with enhanced dynamics of grid-forming converters during fault conditions. IEEE J. Emerg. Sel. Top. Power Electron. 8 (2), 1062–1073.
Tielens, Pieter, Van Hertem, Dirk, 2016. The relevance of inertia in power systems. Renew. Sustain. Energy Rev. 55, 999–1009.
Unruh, Peter, Nuschke, Maria, Strauß, Philipp, Welck, Friedrich, 2020. Overview on grid-forming inverter control methods. Energies 13 (10), 2589.
Urdal, Helge, Ierna, Richard, Zhu, Jiebei, Ivanov, Chavdar, Dahresobh, Amir, Rostom, Djaved, 2014. System strength considerations in a converter dominated power system. IET Renew. Power Gener. 9 (1), 10–17.
Wang, Xiongfei, Harnefors, Lennart, Blaabjerg, Frede, 2017. Unified impedance model of grid-connected voltage-source converters. IEEE Trans. Power Electron. 33 (2), 1775–1787.
Wen, Bo, Boroyevich, Dushan, Burgos, Rolando, Mattavelli, Paolo, 2013. Input impedance of voltage source converter with stationary frame linear current regulators and phase-locked loop. In: 2013 IEEE Energy Conversion Congress and Exposition. IEEE, pp. 4207–4213.
Wen, Bo, Boroyevich, Dushan, Burgos, Rolando, Mattavelli, Paolo, Shen, Zhiyu, 2015. Analysis of DQ small-signal impedance of grid-tied inverters. IEEE Trans. Power Electron. 31 (1), 675–687.
Wu, Heng, Wang, Xiongfei, 2020. Passivity-based dual-loop vector voltage and current control for grid-forming VSCs. IEEE Trans. Power Electron..
Yu, Mengran, Dyśko, Adam, Roscoe, Andrew, Booth, Campbell, Ierna, Richard, Urdal, Helge, Zhu, Jiebei, 2015. Effects of swing equation-based inertial response (SEBIR) control on penetration limits of non-synchronous generation in the Gb power system. IET Conf. Publ. 2015 (CP679).
Zarei, Seyed Fariborz, Mokhtari, Hossein, Ghasemi, Mohammad Amin, Peyghami, Saeed, Davari, Pooya, Blaabjerg, Frede, 2019. Control of grid-following inverters under unbalanced grid conditions. IEEE Trans. Energy Convers. 35 (1), 184–192.
Zhang, Lidong, 2010. Power System Stability Analysis Using Feedback Control System Modeling Including HVDC Transmission Links (Ph.D. thesis). Royal Institute of Technology, Stockholm,Sweden.
Zhang, Weiyi, Remon, Daniel, Rodriguez, Pedro, 2017. Frequency support characteristics of grid-interactive power converters based on the synchronous power controller. IET Renew. Power Gener. 11 (4), 470–479.
Zhong, Qing-Chang, Hornik, Tomas, 2012. Synchronverters: Grid-Friendly Inverters That Mimic Synchronous Generators. Wiley-IEEE Press.
Zhong, Qing-Chang, Weiss, George, 2010. Synchronverters: Inverters that mimic synchronous generators. IEEE Trans. Ind. Electron. 58 (4), 1259–1267.